A COMPLETE Survey of Velocity Features in Perseus

Michelle A. Borkin

Senior Thesis
Astronomy Department, Harvard College

May 2006
Advisor: Prof. Alyssa A. Goodman

Abstract

Using ^{12}CO and ^{13}CO molecular line maps of the Perseus star forming region from the COMPLETE Survey of Star Forming Regions, a catalog of velocity features was compiled using a variety of visualization techniques to identify outflows. 3D isosurface models were generated in RA-DEC-Velocity space using 3D Slicer, a brain imaging and visualization computer application developed at Brigham and Women's Hospital's Surgical Planning Lab, and the high velocity gas features were identified. This visualization allowed for a rapid review of a large area (over 8 square degrees). A total of 217 high velocity (at least 2σ from the peak emission) points were marked in 3D Slicer for all of Perseus. Three regions (B5, IC 348, and L1448) were investigated further to determine which points were associated with known or potentially new outflows. All known outflows in Perseus were detected, 20 points were identified in these three regions as possibly being associated with an undocumented outflow, 3 points were identified with a shell and outflow around B5 IRS4, and 6 points were identified with a possible large shell spanning across the L1448 and NGC 1333 regions of Perseus.

The B5 region was further investigated to determine the mass, momentum, and kinetic energy of the region and of the outflows. The high velocity gas detected from outflowing gas in the B5 region accounts for about 10% of all the high velocity gas in the region. Detected outflows are not the only source of the observed high velocity gas in the region, implying that most of this gas is from undetected outflows, from outflowing gas where the source has stopped producing new outflowing gas, or from some other unexplained turbulent process. The implications of this and future follow-up on this outflowing gas gives insight into where high velocity gas comes from in star forming regions, and the distribution and density of star forming regions.

1. Introduction

1.1 Project Motivation

1.1.1 Astronomical Motivation

The research for this paper was primarily motivated by the desire to study the velocity features of star forming regions over a very large area to gain perspective of large scale trends and statistics. The COMPLETE (CoOrdinated Molecular Probe Line Extinction Thermal Emission) Survey of Star Forming Regions[1] was created with the goal of gaining a better understanding of star formation by studying all of Perseus, Ophiuchus, and Serpens with molecular line, dust emission, and extinction data. This wealth of data allows one to fully study the region and calculate the same properties of the cloud in many different ways.

The molecular line data allows one to directly investigate the velocity structure of a cloud. Each cube is a series of RA-DEC intensity maps (better known as channel maps since there is one for each velocity channel observed by the radio telescope) for a series of velocity values and each map is representative of the emission from the cloud at that particular velocity. The velocity structure describes the kinematics of the gas in the cloud and one is able to see signs of phenomena such as turbulence, expanding shells, and outflows. Understanding how much mass and energy these contribute to the cloud allow provide implications as to the evolution of the cloud, and how active the star formation is in the cloud.

A primary focus of this paper is studying outflows. Outflows are observed across the entirety of Perseus and allow one to identify the location of young stars (less than 10^7 years old) and where active star formation is occurring. When stars form from collapsed gas, matter goes into the core from the accretion disk and at the same time mass is pushed out through bipolar outflows as shown in Figure 1 (Arce 2001). Understanding this outflow phase of a young star is important because the process dissipates extra angular momentum in the system and the outflow can stop the accretion of mass onto the star by blowing away the surrounding material (Arce 2001). It is also the case that the high velocities and energies that are output by the outflow affect the surrounding cloud and is a source of internal energy for it (Margulis & Lada 1985). Knowing where outflows are located within a cloud identify the locations of young stars and where active star formation is occurring, and the study of these outflows is integral to understanding the evolution and velocity distribution of molecular clouds.

[1] http://www.cfa.harvard.edu/COMPLETE

This paper follows a similar approach to that used by Margulis & Lada (1985) where they examined 6 specific outflows. The outflows were observed in ^{12}CO and ^{13}CO, and their masses and energies were calculated. As they state in their discussion, "No systematic search of a single cloud for high-velocity flows has yet been made. Such a study would be valuable, both from the points of view of cloud dynamics and bipolar flow statistics." The research presented in this paper is the first step to study many outflows over a large scale to better understand outflow and cloud dynamics.

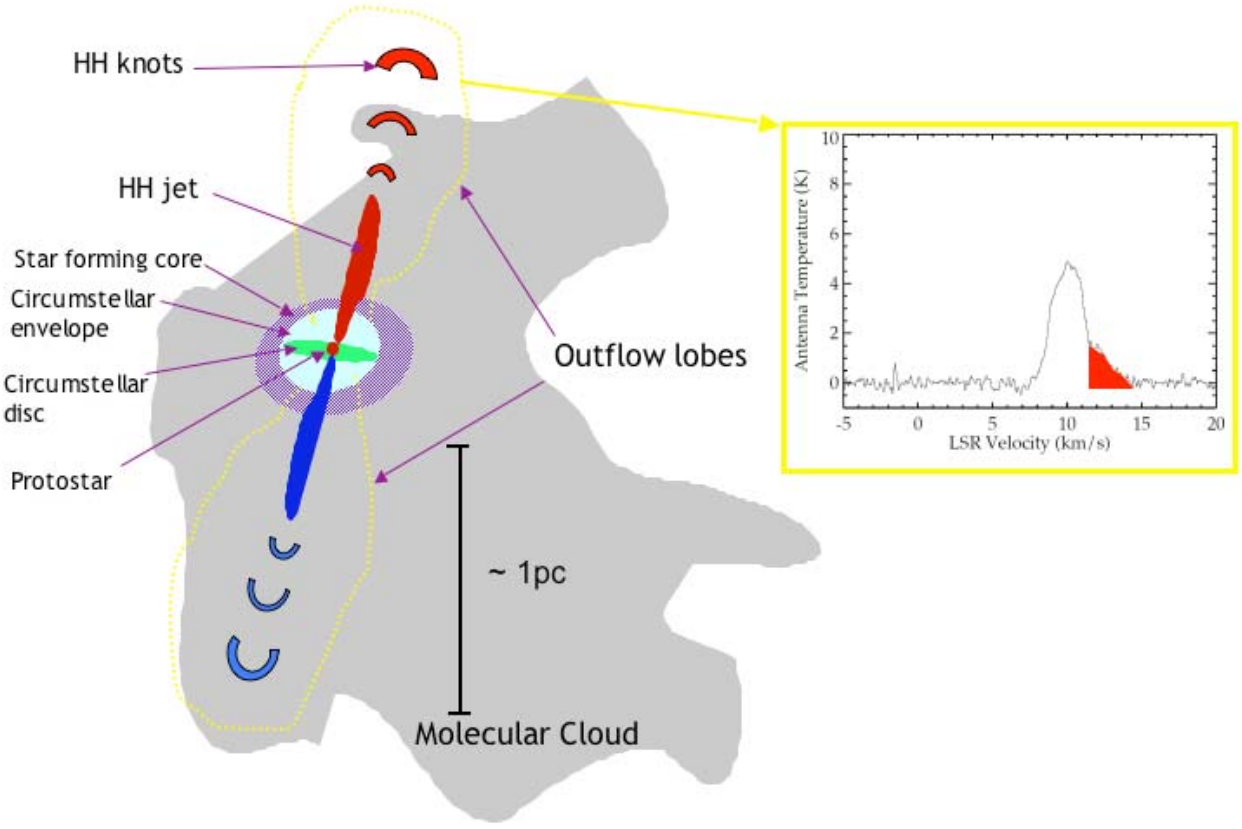

Note: Not drawn to scale.

Figure 1: Schematic depiction of an outflow in a molecular cloud with a sample observation (from B5) of how a red outflow lobe appears in a spectrum as a red velocity wing (based on Figure 1.2 of Arce 2001).

1.1.2 Computational and Analytical Motivation

Another component of this research was to test the effectiveness of using 3D visualization of molecular clouds in RA-DEC-Velocity space to identify velocity features such as outflows. This was inspired by the work done in Borkin et al. 2005 and the Astronomical Medicine (AstroMed) project at the Harvard Initiative in Innovative Computing (IIC)[2]. The goal of the AstroMed project is to address, in both the fields of medical imaging and astronomy, key research challenges including imaging and accessibility of large varying kinds of data. This project takes advantage of medical imaging tools such as 3D Slicer[3] and OsiriX[4] to bring new insight to astronomical data. The primary program used for this research was 3D Slicer which was developed originally at the MIT Artificial Intelligence Laboratory and the Surgical Planning Lab at Brigham and Women's Hospital. It was designed to help surgeons in image-guided surgery, to assist in pre-surgical preparation, to be used as a diagnostic tool, and to help in the field of brain research and visualization as shown in Figure 2 (Gering 1999). 3D Slicer was first used with astronomical data in Borkin et al. 2005 to study the hierarchical structure of star forming cores and velocity structure of IC 348 in ^{13}CO and C^{18}O, and is applied in this paper to all of Perseus.

Visualizing the velocity structure of a cloud in 3D has the advantages of being easier to understand and interpret as compared to channel maps. Traditionally, one has to look through the channel maps one by one (usually in a movie format) or use position-velocity diagrams to construct a 3D interpretation. The creation of a 3D model in essence displays all the maps at the same time by stacking them all together and drawing a 3D surface around the emission. As will be discussed in Section 3, physical phenomena like outflows are easily detectable in the form of spikes. Conventionally outflows are detected by either looking through channel maps for a blue shifted outflow lobe at a low velocity range as compared to the local standard of rest velocity (LSR), and a red shifted lobe at a higher velocity range as compared to the LSR. 3D modeling lets you see all the velocity values at the same time so blue and red shifted lobes are concurrently visible. The other way to find outflows is to individually examine known young stars in a region and observe them to see if they have an outflow. This is inefficient since not all young stars have

[2] http://iic.harvard.edu

[3] http://www.slicer.org/

[4] http://homepage.mac.com/rossetantoine/osirix/

outflows. The 3D modeling used in this paper proved to be an excellent and efficient way to identify outflows, particularly over a large area such as Perseus which is 8.7 square degrees.

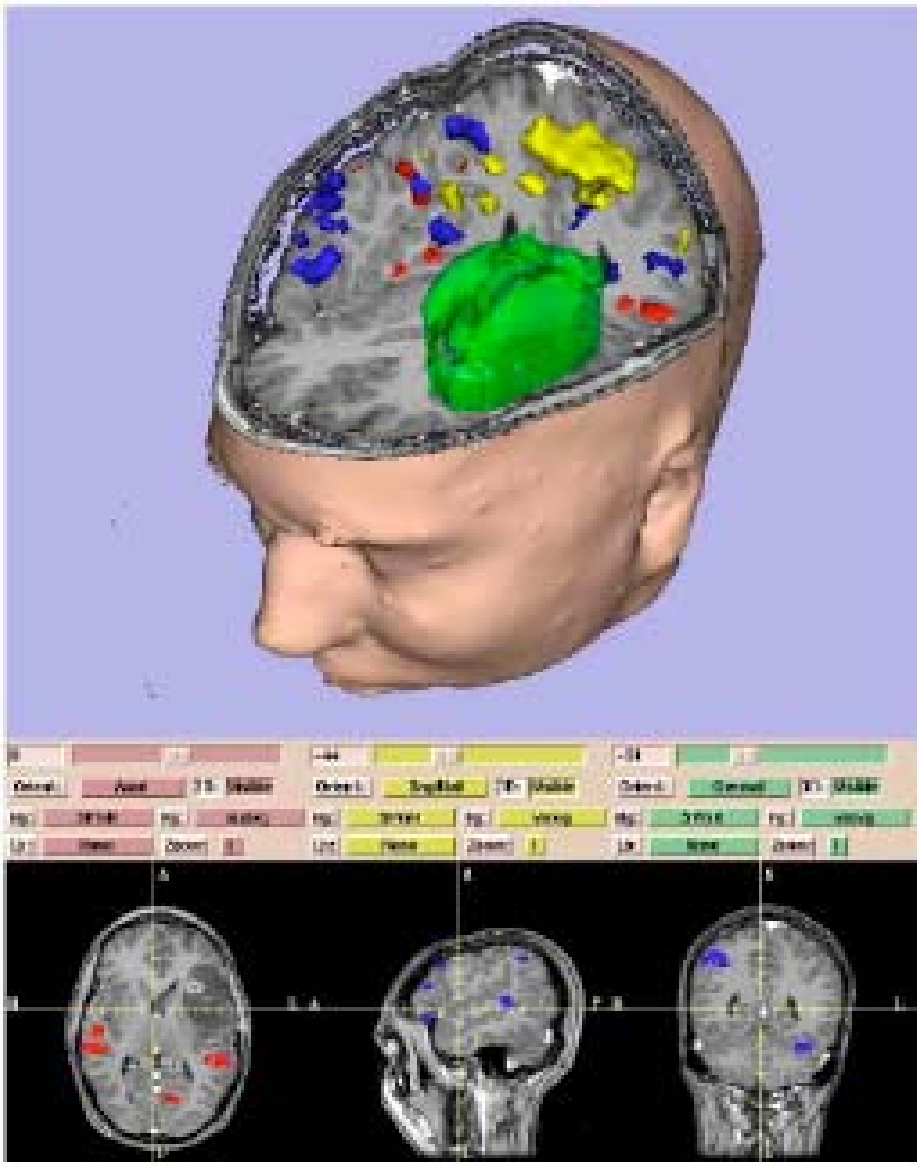

Figure 2: Screen shot of 3D Slicer displaying a tumor (green) in an MRI scan of a brain. (From Gering, et al. 1999)

1.2 Background on Perseus

Perseus is a chain of molecular clouds at a distance of 250±50 pc, is about 10^4 $M_\odot$, and encompasses a total area of about 70 pc^2 (Enoch, et al. 2006). It should be noted that there is a range of distance estimates from 230 pc (Cernis 1990) to 350 pc (Herbig & Jones 1983). This variation is due to the fact that there are multiple cloud components along the line of sight at different distances making a single distance estimate to Perseus difficult to determine. Perseus contains multiple young active star forming regions including IC 348 and NGC 1333, and other areas of interest including B5, B1, L1448, and L1455. There have been many surveys of the region that have found a large population of pre-main sequence stars throughout the region (Ladd et al. 1993; Aspin et al. 1994; Lada & Lada 1995; Luhman et al. 2003) but few high-mass stars. The whole Perseus region was first surveyed in ^{12}CO by Sargent (1979). For this paper, ^{12}CO and ^{13}CO data collected on Perseus as part of the COMPLETE Survey is used (Ridge et al. 2006). The COMPLETE Survey chose in part to map Perseus because it is one of the regions covered in the Cores to Discs (c2d) Spitzer Legacy Project[5]. Perseus was observed with multiple instruments on Spitzer including IRAC and MIPS (Jørgensen et al. 2006).

2. Data

The ^{12}CO and ^{13}CO molecular line map data was collected between 2002 and 2005 using the 14-meter FCRAO (Five College Radio Astronomy Observatory) telescope with the SEQUOIA 32-element focal plane array. The receiver was used with a digital correlator providing a total bandwidth of 25 MHz over 1024 channels. The ^{12}CO J=1-0 (115.271 GHz) and the ^{13}CO J=1-0 (110.201 GHz) transitions were observed simultaneously using an on-the-fly mapping technique (OTF) (Ridge, et al. 2006). CO is a good tracer for studying molecular clouds because ^{12}CO will show the outer part of the cloud while ^{13}CO will show the denser regions where ^{12}CO is optically thick. Observations were made in 10 x 10 arcminute maps with an effective velocity resolution of 0.07 km s^{-1} and these were then patched together to form the entire Perseus region as shown in Figures 3 and 4. Using IDL, a series of 472 RA-DEC Perseus map slices were put together representing the velocity range of -5 to 25 km s^{-1}. Each of these map slices is a single 0.07 km s^{-1} velocity channel. The cube was then filtered by removing noisy pixels (pixels that were 3 times the average rms noise for the cube) and then smoothing the

[5] http://peggysue.as.utexas.edu/SIRTF/

cube by a factor of 2 in all three dimensions (RA, DEC, and velocity).

For analysis purposes, Perseus was divided into six regions as shown in Figure 5. Due to the velocity gradient across the whole Perseus region, it was necessary to divide it into smaller regions with similar LSR velocities. This allowed for easier visualization of the 3D models since they would appear more square (discussed in section 3.1). The borders of these regions were chosen based on aesthetics and a desire to encompass specific star forming regions. The regions overlap by either 20 or 50 pixel margins to guarantee complete analysis. For each of these six regions, the data cube was converted into a series of TIFF grayscale images (one for each channel map) in order to be read into 3D Slicer.

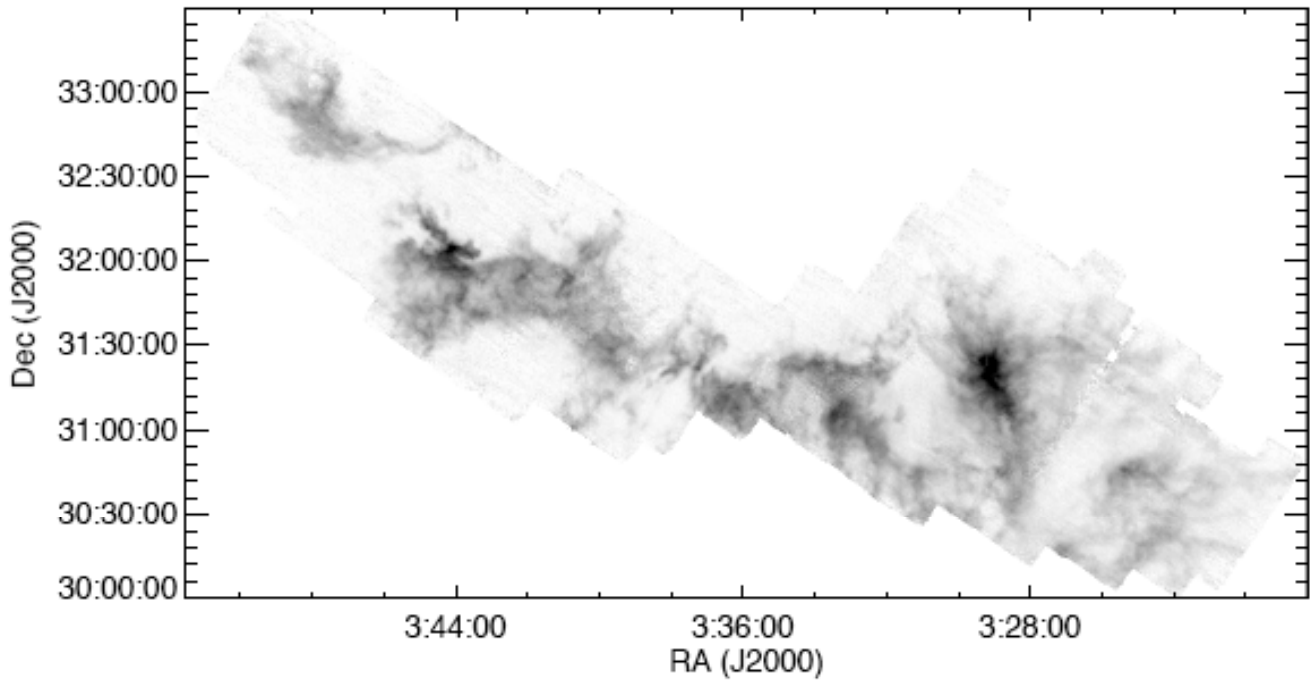

Figure 3: Integrated map of Perseus in ^{13}CO

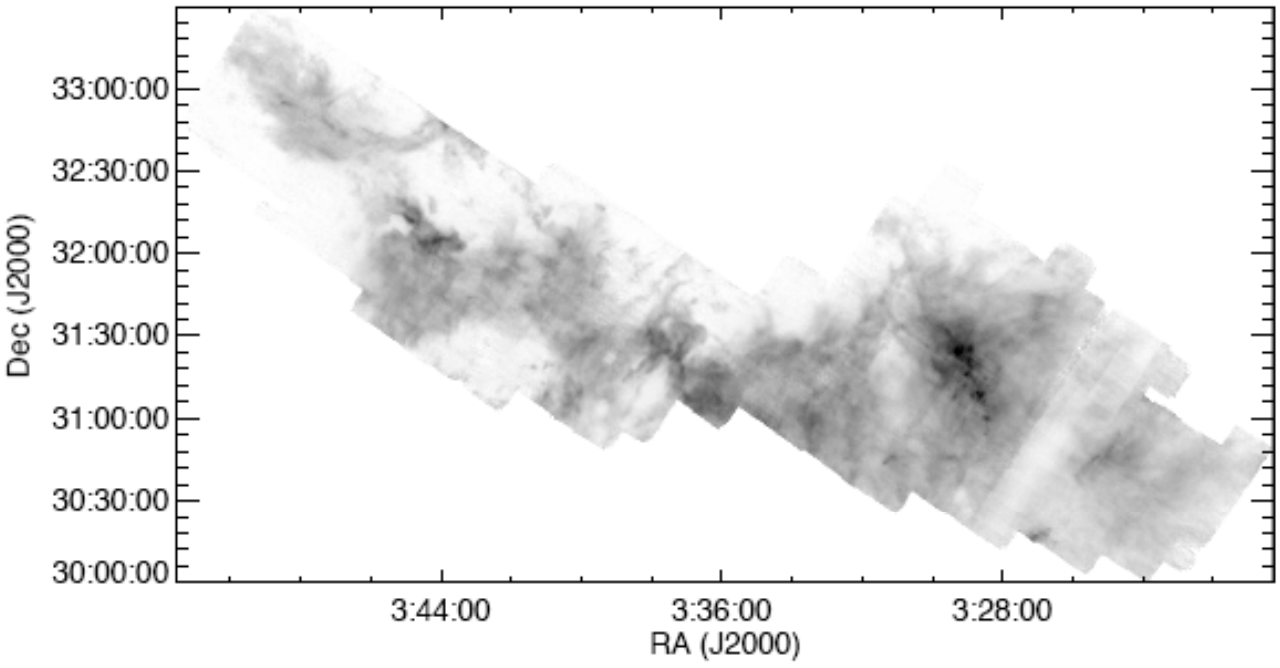

Figure 4: Integrated map of Perseus in ^{12}CO

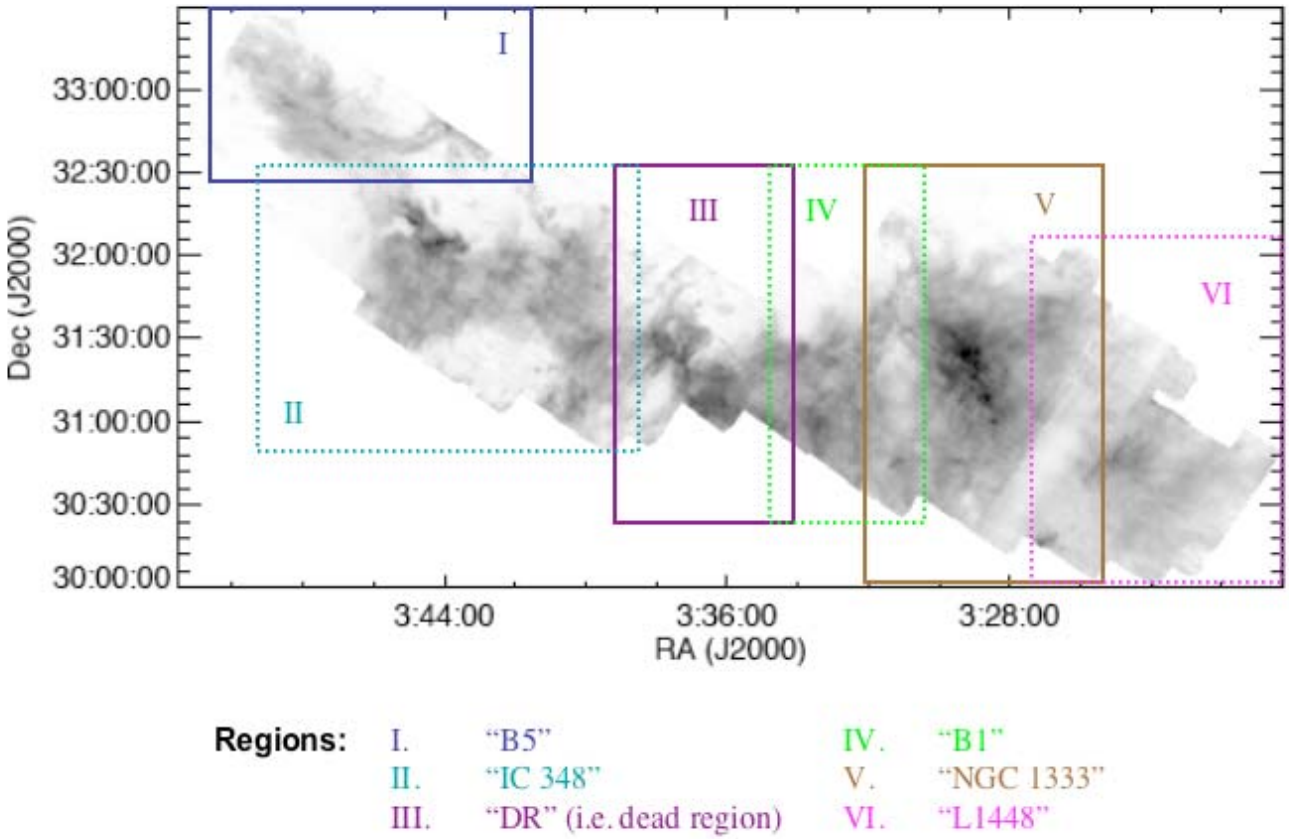

Figure 5: Perseus region boundaries overlaid on a ^{12}CO integrated map of Perseus (see Table A1 in the Appendix for the specific corner coordinates).

3. Analysis

3.1 3D Slicer Models

For each region of Perseus (see Figure 5), an isosurface (constant intensity level) model was generated in 3D Slicer. The threshold (i.e. emission intensity level) for each model was chosen to be the lowest level of emission above the rms noise level for that particular region. For the specific settings used to make each model, see Table A2 in the Appendix. Thus, in ^{12}CO this would create a 3D model representing all of the detected emission. 3D Slicer allows one to interactively manipulate the model and visualize the velocity structure of the gas.[6] The outflowing gas in this 3D space can be identified in the forms of spikes, as shown in Figure 6, which visually stick out from the general distribution of the gas. These spikes occur since one is looking at the radial velocity component of the gas along the line of sight, thus causing the sharp spikes along the line of sight where ever there is high velocity (at least 2σ from the peak emission) gas.

Once the 3D model had been created, the spikes can be visually marked with fiducial points (the green markers in Figure 6). The points were marked on the cube systematically by viewing the cube from every possible orientation. The ability of sliding channel maps through the cube proved to be a helpful check to make sure that the emission looked real. A total of 216 points were identified and are listed in Table A3 of the Appendix. The locations of all the high velocity points in the 3D space were recorded by 3D Slicer in an xml text file. From this file, the pixel coordinates were extracted and converted to astronomical coordinates with the WCSTools package. A list of all the high velocity points identified in 3D Slicer is in Table A3. Instead of having to go through each region and carefully examine each channel map, or randomly scroll through the spectra by hand as described in Section 1.1.2, 3D Slicer allows one to instantly see where the high velocity points are located, and then further examine them in conventional astronomical applications such as DS9[7], Aipsview[8], or Karma[9] which are capable of understanding astronomical coordinates, displaying spectra, and more easily overlaying multiple astronomical images.[10]

---

[6] For a movie demonstrating astronomy data in 3D Slicer, go to http://www.cfa.harvard.edu/COMPLETE/astromed/

[7] http://hea-www.harvard.edu/RD/ds9/

[8] http://aips2.nrao.edu/aips++/docs/user/Aipsview/Aipsview.html

[9] http://www.atnf.csiro.au/computing/software/karma/

[10] The IIC and SPL are currently working to create a new version of 3D Slicer that will have all of these capabilities.

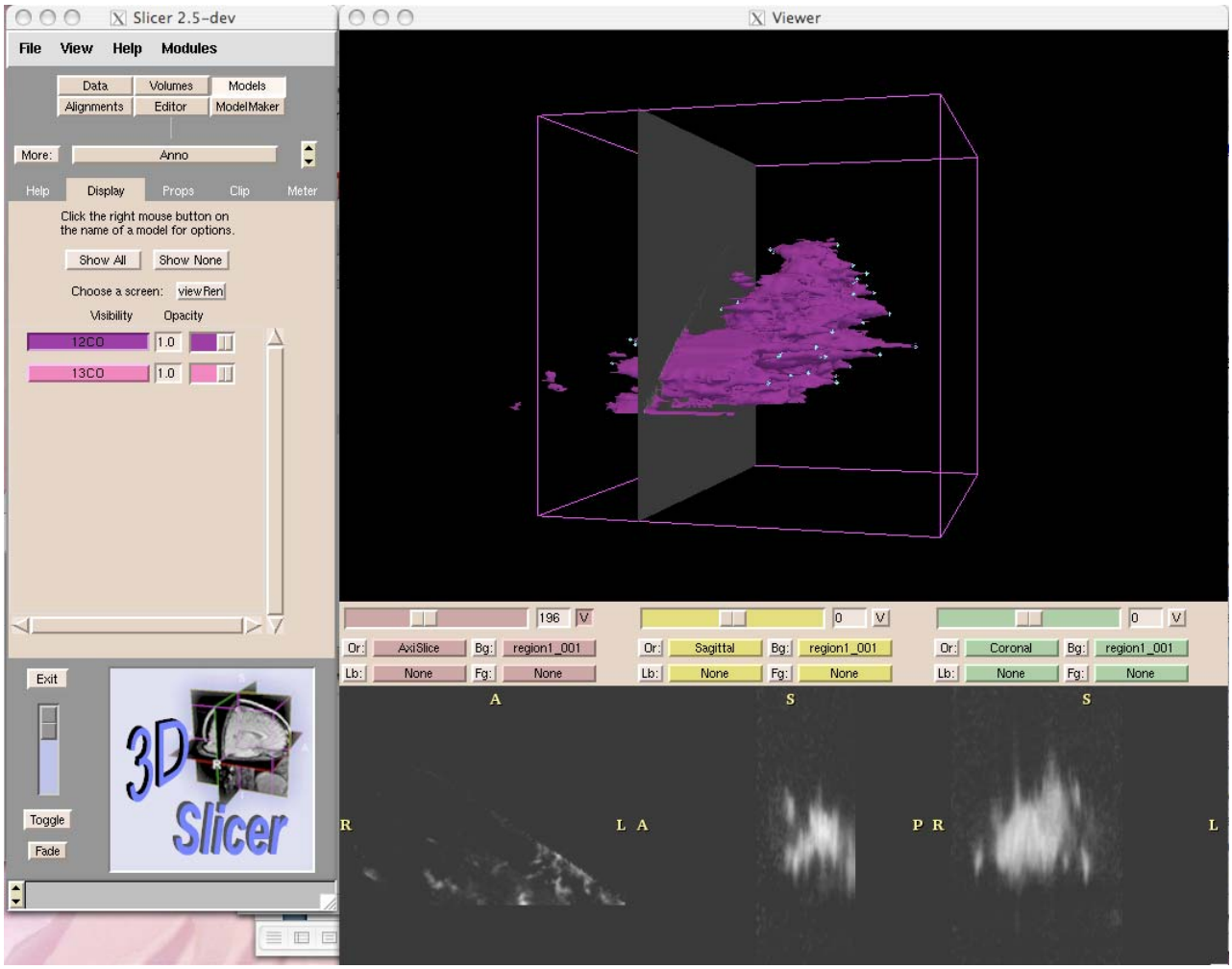

Figure 6: Screen shot of the ^{12}CO surface model for Region 1 with a channel map and fiducial points marking the high velocity peaks.

3.2 Outflow Identification

In order to determine if the specific points marked in 3D Slicer are associated with an outflow, the individual spectra for each point and their location relative to known outflow sources, IRAS sources, c2d sources, and HH objects were examined. The first step was to take the 3D Slicer points and overlay them onto the ^{12}CO data cube in Aipsview. The points' coordinates along with the coordinates for known IRAS sources, known outflows (taken from Wu, et al. 2004), and HH objects in Perseus were put into an Aipsview overlay file as shown in Figure 7. These points and the location of c2d sources are overlaid on a Spitzer IRAC image in Figure 8. (The c2d sources included in the overlay file came from Tom Laakso's Senior Thesis.) They represent a minimal list of confirmed young sources. Also included in the overlay are the positions of potential outflows as identified with the Spectral Correlation Function (SCF) (Rosolowsky, et al. 1999; Fallscheer, et al. 2003). With the aid of this overlay file and the examination of each spectra, it can be decided whether the point is a random bad pixel, is associated with an outflow or shell, or is due to some other turbulent process.

This analysis was conducted for Regions 1, 2, and 6 (see Figure 5). These regions were chosen due to their relative simplicity compared to the others and these comprised of already well studied outflow regions. Even though each high velocity point is a coordinate for a single pixel where the marker was placed on the model in 3D Slicer, it identifies a small area of high velocity gas. In Table 1, for each point identified by 3D Slicer in these regions there is a velocity range for the gas (determined by looking at the wing of the spectrum), and any potential source associations. This list also identifies which points are associated with known outflows, are possibly associated with undocumented outflows, or are associated with expanding shells. The number of points associated with a single outflow varies. For example, the B5 outflow is identified by 6 points, L1451 by 3 points, and the individual outflows in IC 348 and NGC 1333 by 1 point each. A single point can either represent a whole lobe, or a piece of gas along a large outflow lobe. From the analysis conducted so far, aside from the very large outflows (like B5) a typical outflow is identified by 1 or 2 points. Table 2 shows the number of points per outflow for Regions 1, 2, and 6.

Table 1: Catalogs for Regions 1, 2, and 6. Blue highlights for known outflows, pink highlights for suspect outflows, and yellow highlighs for shell associations.

	ASTRONOMICAL (RA,DEC)												
	J2000			J2000			Velocity Range		Bad	NEARBY OBJECTS			
name	RA			DEC			min (km/s)	max (km/s)	Pixel	IRAS	HH	c2d	SCF
region1_B0	3	42	56.897	32	41	19.26	5.968	6.603					
region1_B1	3	50	0.465	32	58	21.73	8.382	8.763					
region1_B2	3	49	40.917	33	1	18.97	9.017	9.715					
region1_B3	3	49	23.079	33	2	20.31	7.747	8.509					(57.355 33.04917) questionable
region1_B4	3	48	18.933	32	54	55.1	6.286	8.255			LOTS		
region1_B5	3	48	9.68	32	33	53.85	6.73	8.001					
region1_B6	3	44	24.148	32	47	24.59	6.349	7.175					
region1_B7	3	44	12.554	32	49	3.46	5.968	6.73					
region1_B8	3	43	54.187	32	49	22.41	7.175	7.683					
region1_B9	3	43	18.17	32	28	17.06	6.286	7.112					
region1_B10	3	43	40.476	32	29	52.22	6.794	7.493					
region1_B11	3	45	15.338	32	29	11.42	6.603	7.302					
region1_B12	3	48	23.89	32	38	43.7	7.239	7.747				J034834.1+323748	
region1_B13	3	47	26.828	32	34	24.27	7.302	7.683					
region1_B14	3	46	35.706	32	27	13.07	7.366	8.001					
region1_B15	3	45	58.399	32	42	31.78	7.112	8.382					
region1_B16	3	44	53.611	32	32	19.87	6.54	7.366					
region1_B17	3	45	46.127	33	0	28.45	8.191	9.144					
region1_B18	3	48	40.355	33	24	40.03	9.017	9.461					
region1_B19	3	48	34.518	33	23	19.24	9.017	9.588					
region1_B20	3	46	39.406	32	44	49.1	7.493	8.572					
region1_B21	3	48	57.95	32	52	47.23	8.255	8.636					
region1_B22	3	49	44.549	33	12	34.41	8.572	9.017					
region1_B23	3	44	47.761	32	38	26.03	7.302	7.683					
region1_B24	3	47	24.118	33	3	7.11	8.445	8.953		IRS 4	a few		
region1_R0	3	47	0.942	32	46	24.31	11.43	13.02		IRS 1, IRS 3	lots	J034656.7+325248	
region1_R1	3	46	37.84	32	43	34.3	11.68	13.46		IRS 1, IRS 3			
region1_R2	3	46	1.162	32	33	35.49	11.18	11.62		IRS 1?		J034607.4+323308	(56.46167 32.59556) good candidate
region1_R3	3	46	5.65	32	52	6.46	11.3	11.81					
region1_R4	3	43	46.851	32	47	14.48	10.29	11.56					
region1_R5	3	44	35.12	32	43	23.16	11.18	11.62					
region1_R6	3	47	18.211	32	38	41.2	11.56	12		IRS 3	a few	J034715.2+323706	
region1_R7	3	47	19.34	32	58	36.93	12.32	13.08			a few		
region1_R8	3	48	9.963	33	14	19.86	11.56	12.26					
region1_R9	3	49	9.344	33	18	1.36	11.3	11.62					(57.27 33.33028) questionable, (57.23208 33.26) good candidate
region1_R10	3	47	3.748	32	55	16.88	11.75	12.32				J034656.7+325248	
region1_R11	3	50	11.697	33	7	5.57	11.56	12					
region1_R12	3	47	3.007	32	35	10.48	10.92	11.3				J034651.5+323226, J034715.2+323706	
region1_R13	3	49	19.173	32	57	19.33	10.35	11.18					
region1_R14	3	47	53.633	33	1	54.34	11.56	12.06		IRS 4			
region1_R15	3	49	21.174	33	26	32.4			X				
region1_R16	3	50	5.948	33	9	58.34	11.24	11.81					
region1_R17	3	47	26.518	32	49	46.41	11.3	12.13		IRS 1			
region1_R18	3	47	34.82	33	6	24.22	11.24	11.81		IRS 4			
region1_R19	3	49	27.864	33	12	31.22	11.37	11.68					
region1_R20	3	48	34.244	32	58	24.19	11.43	13.91		IRS 1			
region1_R21	3	45	32.974	32	43	11.93	11.05	11.62					
region1_R22	3	44	5.616	32	43	43.26	10.03	10.54					
region1_R23	3	43	32.194	32	36	57.21	9.779	10.79					
region1_R24	3	42	56.459	32	35	20.47	9.652	10.73					
region1_R25	3	43	10.799	32	37	41.53	10.1	11.37					
region1_R26	3	48	55.315	33	11	3.13	11.43	11.68					
region1_R27	3	45	17.163	32	42	28.52	11.05	11.3					
region1_R28	3	44	58.668	32	37	33.4	10.54	11.05					

region1_R29	3	43	44.945	32	45	1.42	9.842	10.54					
region2_B0	3	43	16.673	31	38	46.31	4.19	5.143					
region2_B1	3	41	24.621	31	40	1.39	4.952	5.524					
region2_B2	3	40	18.714	31	15	29.91	2.92	4.889				a few	
region2_B3	3	39	42.569	30	54	37.36	0.6978	2.095					
region2_B4	3	41	0.652	31	8	49	4.063	5.714					
region2_B5	3	41	41.337	31	26	52.52	5.079	5.714					
region2_B6	3	41	52.472	31	33	10.56	4.952	5.46					
region2_B7	3	41	59.409	31	31	51.28	5.016	5.714					
region2_B8	3	44	3.18	32	5	10.86	5.968	6.603			lots	lots, J034359.9+320441	
region2_B9	3	45	25.467	31	48	4.37	4.762	5.333				J034533.5+314555	
region2_B10	3	45	3.679	32	0	21.59	5.397	5.714				lots	
region2_B11	3	44	48.531	31	33	11.26	3.492	4.508					03 44 59 +31 29 48 point of interest
region2_B12	3	39	18.147	32	16	59.03	6.476	7.683					
region2_B13	3	43	55.891	32	4	42.35	5.841	6.349			lots	lots	03 43 58.4 +32 05 50 good candidate
region2_B14	3	40	50.732	31	19	36.16	4.571	5.397					
region2_B15	3	45	12.281	32	29	13.08	5.587	6.159				a few scattered	
region2_B16	3	42	28.54	31	36	52.7	5.079	5.46					
region2_R0	3	41	29.777	32	14	31.35	10.22	11.24					
region2_R1	3	44	53.603	32	13	34.54	10.6	11.24				lots	
region2_R2	3	40	22.648	32	3	24.27	10.79	11.94					03 40 34 +32 01 14 questionable
region2_R3	3	39	24.207	31	56	36.79	11.24	11.94		IRAS 03367+3147			
region2_R4	3	39	58.376	31	44	54.57	11.3	12.19					
region2_R5	3	39	33.049	31	29	59.68	11.37	12.38					
region2_R6	3	41	1.838	31	33	42.82	11.37	12.13					03 40 52.3 +31 28 16 questionable
region2_R7	3	44	13.413	31	26	58.98	11.05	11.68					
region2_R8	3	44	37.648	31	57	48.08	10.48	11.3				many, J034432.6+320856	
region2_R9	3	42	12.374	31	51	7.83	11.11	11.75				many	
region2_R10	3	41	40.606	32	1	12.63	11.18	11.62					03 41 28.6 +32 01 14 point of interest
region2_R11	3	39	15.64	31	19	9.22	12.51	11.37				J033910.5+312025	
region2_R12	3	45	55.721	32	33	1.61	10.86	11.62				J034607.4+323308	
region2_R13	3	45	42.364	31	41	6.48	10.79	11.49				J034533.5+314555	
region2_R14	3	45	22.937	31	56	28.46	11.11	11.43				lots, J034518.3+315426	
region2_R15	3	41	27.266	32	15	48.04	10.29	11.43					
region2_R16	3	43	56.815	32	2	10.57	10.35	11.24			lots	lots	
region2_R17	3	39	34.339	31	38	47.79	11.24	11.56					
region2_R18	3	45	7.453	31	57	32.3	10.6	11.18					
region6_B0	3	23	7.046	30	59	17.06	-2.668	-1.271					
region6_B1	3	25	6.195	31	14	53.08	-1.652	-1.207					
region6_B2	3	25	24.075	31	19	29.75	-1.652	-1.144					
region6_B3	3	26	47.701	30	16	58.91	0.3803	2.666		L1451	lots		
region6_B4	3	22	10.514	30	47	55.03	-1.715	-1.207					
region6_B5	3	26	35.315	30	18	21.94	-0.1912	2.793		L1451	lots		
region6_B6	3	24	52.887	30	42	17.89	-1.207	-0.6993		L1448 IRS1			
region6_B7	3	21	46.428	30	37	55.87	-1.207	-0.4453					
region6_B8	3	21	13.402	30	35	15.28	-0.8898	-0.5088					
region6_B9	3	23	31.955	30	25	19.91	0.3803	1.015					
region6_B10	3	22	54.28	30	6	18.76			X				
region6_R0	3	26	55.727	30	17	0.42	7.62	10.79		L1451	lots		
region6_R1	3	23	54.208	30	3	29.91	6.603	7.175					
region6_R2	3	25	28.829	30	41	28.48	7.747	10.67		L1448 (multiple)			
region6_R3	3	25	41.325	30	38	38.29	7.493	9.334		L1448 (multiple)			
region6_R4	3	24	16.837	30	50	13.6	7.81	8.445			HH 268		
region6_R5	3	23	4.272	31	3	9.4	6.667	7.683					
region6_R6	3	23	25.714	30	50	6.35	7.62	8.318					
region6_R7	3	25	16.832	30	44	31.24	7.493	9.969		L1448 (multiple)			
region6_R8	3	27	19.493	30	32	51.48	7.366	8.001					
region6_R9	3	26	43.679	31	17	8.79	8.509	9.461					

Table 2: Number of 3D Slicer points per ouflow feature or region.

Feature	**Number of high velocity points**
B5 IRS1 outflow	6
B5 IRS3 outflow	2
B5 IRS4 outlfow/shell	3
region1_B22 and region1_R19	2
region1 non-associated points	6
IC 348 core outflows	3
region2 non-associated points	10
L1451	3
L1448	3
region 6 non-associated points	2
total points for unknown outflows:	20

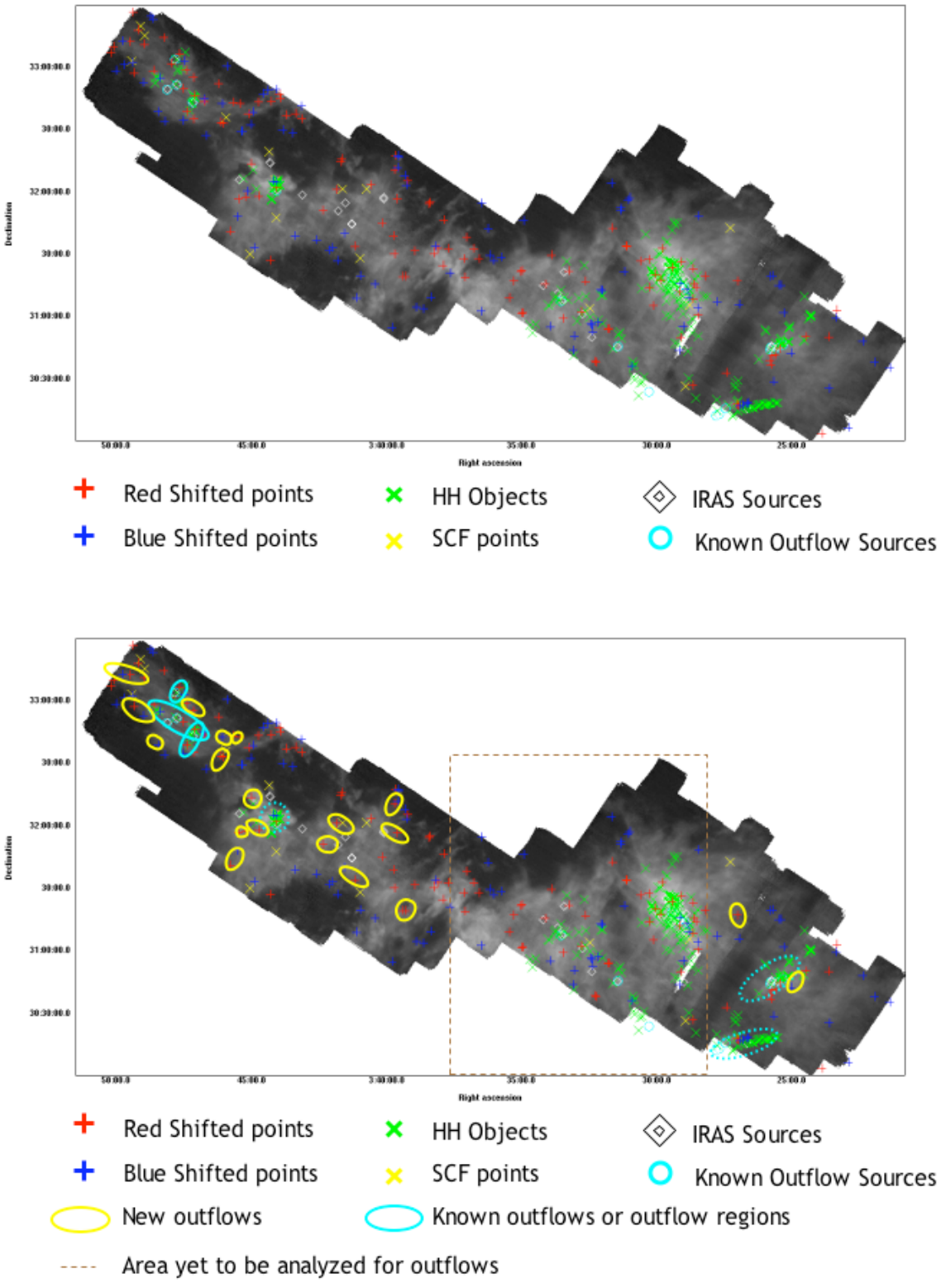

Figure 7: Top panel – integrated ^{12}CO molecular line map with 3D Slicer velocity points, SCF identified regions, IRAS sources, and known outflow sources. Bottom panel – same as top, but with identified outflows and area yet to be analyzed for outflows.

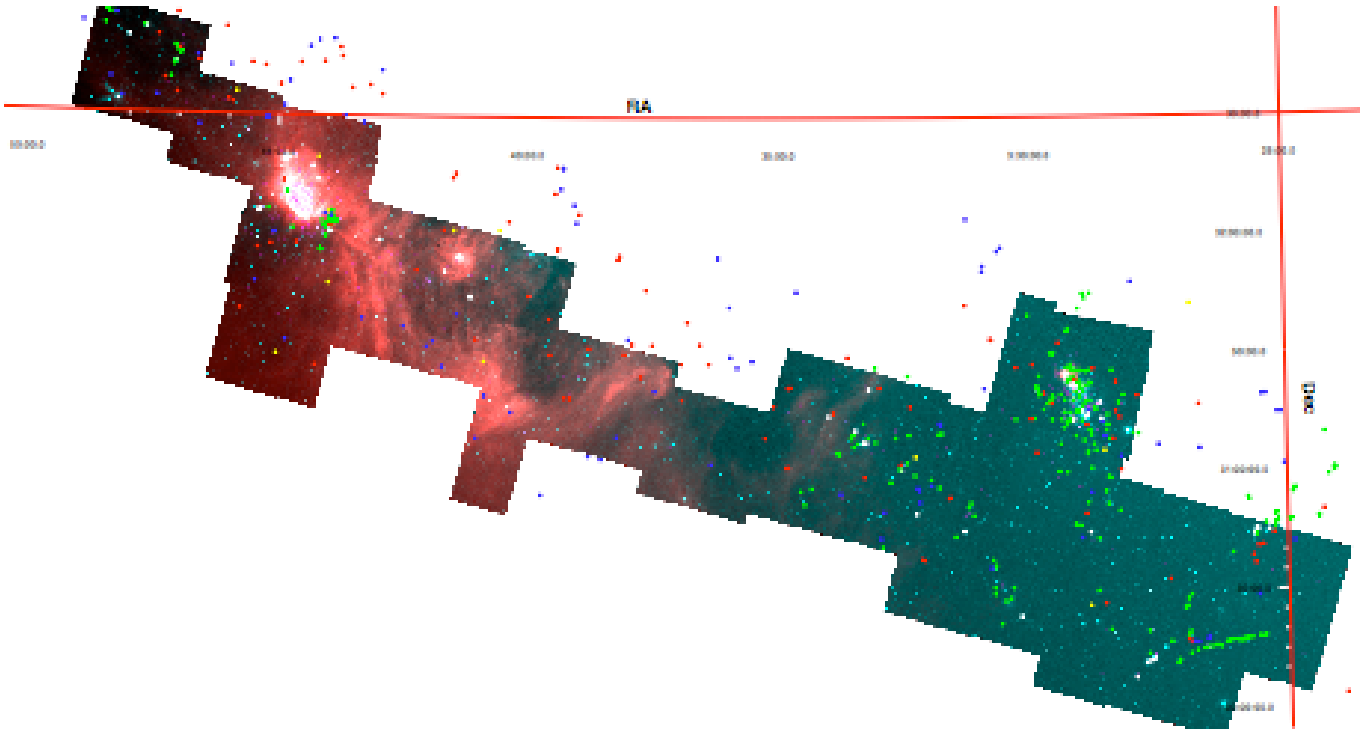

Figure 8: Overlay of points from Figure 7 and young c2d sources (pink boxes) onto a Spitzer IRAC image of Perseus. (A high resolution version of this figure can be downloaded at http://www.cfa.harvard.edu/COMPLETE/astromed/borkin_Figure8.pdf)

3.3 B5 Detailed Calculations

For Region 1 (B5), more careful analysis was conducted in order to calculate the total mass, momentum, and kinetic energy associated with the points identified as being part of outflows. Since CO is a diatomic rotational molecule, observations of its emission allows one to make the following calculations. Assuming local thermodynamic equilibrium (LTE), one can obtain the column density:

$$N_{tot} = \frac{3k}{\left(8\pi^3 B\mu^2\right)} \cdot \frac{\exp\left(hBJ\left(J+1\right)/kT_{ex}\right)}{J+1} \cdot \frac{T_{ex} hB/3k}{1-\exp\left(-h\nu/kT_{ex}\right)} \cdot \int \tau_\nu d\nu \qquad (1)$$

where B is the rotational constant of the molecule, μ (CO's permanent dipole moment) is 0.112 Debye, k is the Boltzmann constant, h is the Planck constant, J is the quantum number of the angular momentum, $\tau_\nu = \tau(\upsilon)$ which is the optical depth as a function of frequency, and T_{ex} is the excitation temperature.[11] This simplifies for ^{12}CO to:

$$N_{^{12}CO} = \frac{2.31x10^{14}\left(T_{ex}+0.92\right)}{1-\exp\left(-5.53/T_{ex}\right)} \int \tau_{\nu\,^{12}CO}\, d\nu \qquad (2)$$

and simplifies for ^{13}CO to:

$$N_{^{13}CO} = \frac{2.42x10^{14}\left(T_{ex}+0.88\right)}{1-\exp\left(-5.29/T_{ex}\right)} \int \tau_{\nu\,^{13}CO}\, d\nu \qquad (3)$$

It is customary when observing at radio wavelengths to measure the brightness temperature ($T_b(\nu)$). The brightness temperature is useful because in the Rayleigh-Jeans regime this is proportional to the thermodynamic temperature of a black body:

$$T_b\left(\nu\right) = \left(J_\nu\left(T_{ex}\right) - J_\nu\left(T_{bg}\right)\right)\left(1-\exp\left(-\tau_\nu\right)\right) \qquad (4)$$

where:

$$J_\nu\left(T_{ex}\right) = \frac{h\nu/k}{\exp\left(h\nu/kT_{ex}\right)-1} \quad \text{and} \quad J_\nu\left(T_{bg}\right) = \frac{h\nu/k}{\exp\left(h\nu/kT_{bg}\right)-1} \qquad (5)$$

and T_{bg} ~2.7 K (the temperature of the microwave background). Assuming that the excitation temperature is the same for ^{12}CO and ^{13}CO, then:

[11] Equations in the following discussion come from or are based equations in Rohlfs & Wilson "Tools of Radio Astronomy" and Bourke, et. al 1997

$$\frac{T_{b\,^{12}CO}}{T_{b\,^{13}CO}} \sim \frac{1-\exp\left(-a\tau_{13}\right)}{1-\exp\left(\tau_{13}\right)} \tag{6}$$

assuming an isotopic abundance ratio of $\frac{^{12}CO}{^{13}CO} \sim 62$. This equation can be solved for τ_{13} numerically and then substituted back into equation (3). To obtain $N_{^{12}CO}$ in areas where there is no significant contribution from the ^{13}CO gas, the ^{12}CO gas can be approximated as optically thin ($\tau_\nu << 1$):

$$\tau_\nu = \frac{T_{b\,^{12}CO}}{J_\nu\left(T_{ex}\right) - J_\nu\left(T_{bg}\right)} \tag{7}$$

This expression can then be substituted into the equation (2).

To find the excitation temperature (T_{ex}), we can make the approximation that at the ^{12}CO line center, the gas is optically thick ($\tau_\nu >> 1$) thus,

$$T_b = J_\nu\left(T_{ex}\right) - J_\nu\left(T_{bg}\right) \tag{8}$$

and solving this for T_{ex}:

$$T_{ex} = \frac{h\nu / k}{\ln\left(1 + \left(\left(h\nu / k\right) / \left(T_b + J_\nu\left(T_{bg}\right)\right)\right)\right)} \tag{9}$$

To calculate the mass of the gas, the ratio of the column densities of ^{12}CO to ^{13}CO is used:

$$N_{H_2} = N_{CO} X \tag{10}$$

where X is the abundance ratio[12] $\frac{^{12}CO}{H_2} \sim 10^{-4}$. The mass per velocity channel is:

$$\text{Mass}(\nu) = N(\nu)(\text{observed area})(\text{mean molecular mass}) \tag{11}$$

With the mass, the momentum can be calculated as follows:

$$P\left(\nu\right) = M\left(\nu\right)v \tag{12}$$

where v is the velocity. Thus the kinetic energy is:

[12] Abundance ratios taken from Rohlfs & Wilson "Tools of Radio Astronomy"

$$KE(\nu) = \frac{1}{2} M(\nu) v^2 \tag{13}$$

These equations will be used in Section 4.2 to determine the kinematic properties of the B5 region.

4. Results

4.1 Features of the Perseus Star forming Region

4.1.1 Shells

One type of velocity feature that is easily identifiable in RA-DEC-Velocity space is an expanding shell. Figure 9 gives some examples of what the spectra of a shell theoretically and actually look like. The velocity of gas in a shell is directly correlated with its spatial position, so a shell appears as it would if it were in three spatial dimensions. However, since the gas is usually optically thin in these shells, usually only a ring is visible around the edge since there is more gas along the line of sight. When examining Perseus in 3D Slicer or other 3D programs (such as OsiriX), one sees many "holes" in both ^{12}CO and ^{13}CO. Most of these do not appear to be shells since their spectra do not show any velocity signature, and they are not perfectly spherical. One specific region where this is visible is in NGC 1333 as shown if Figure 10. One theory described in Quillen et al. 2005 suggests that these were created by outflows which do not exist anymore. These holes could possibly be due to random gas motions, or possibly due in part to optical depth effects. The fact that these holes appear in the gas structure across all of Perseus is an area for further investigation.

Shells of varying sizes are visible in Perseus. One shell is located around B5 IRS4 (IRAS 03446+3254) in Region 1. This shell is marked in Figure 11 on both ^{12}CO and ^{13}CO integrated maps. This shell was first identified by Goldsmith et al. 1986. Around the shell's edge three points were visible in 3D Slicer – one blue shifted and two red shifted. They line up exactly on the edge of the shell, but it is also the case that the two red shifted points are in line with both IRS4 and HH 845. According to Wu et al. 2004, there is an outflow located within this shell. This would make sense due to the strong spikes visible with it in the ^{12}CO isosurface model, and the atypical spectrum (see Figure 9).

Another possible shell is visible spanning across Regions 5 and 6. This feature is visible in ^{12}CO and ^{13}CO, and is best visualized in OsiriX as shown in Figure 12. This emission originally appeared to be a separate cloud along the same line of sight, however in this 3D representation the emission appears to be continuously connected. Possible phenomena that could cause a shell this large might be a supernova, or radiation wind from a star cluster.

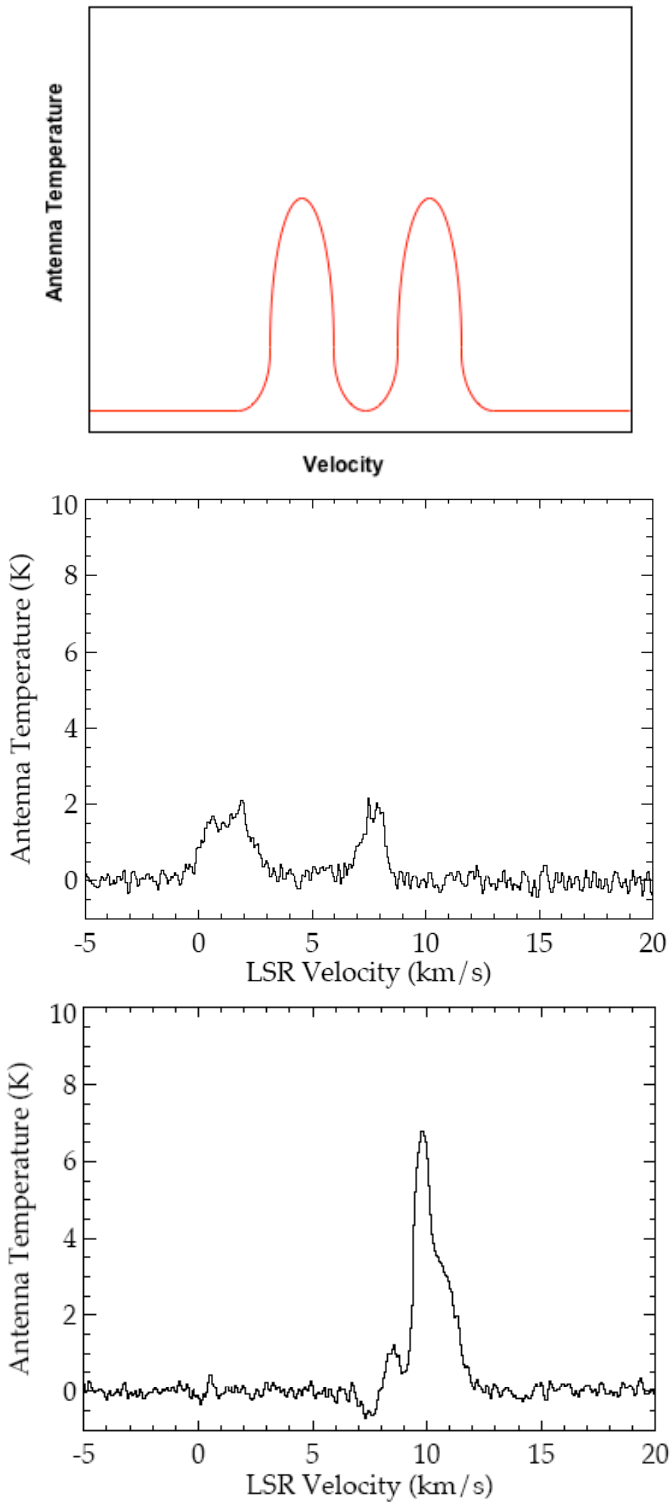

Figure 9: The top panel represents an idealized spectrum of an expanding shell. The two lower panels are integrated ^{12}CO spectra of two shells found in Perseus (middle – large shell spanning Regions 5 and 6, bottom – B5 IRS 4). The bottom spectrum is not like the model spectrum because it has a red wing due to an outflow within the shell and is broad due surrounded by other emission.

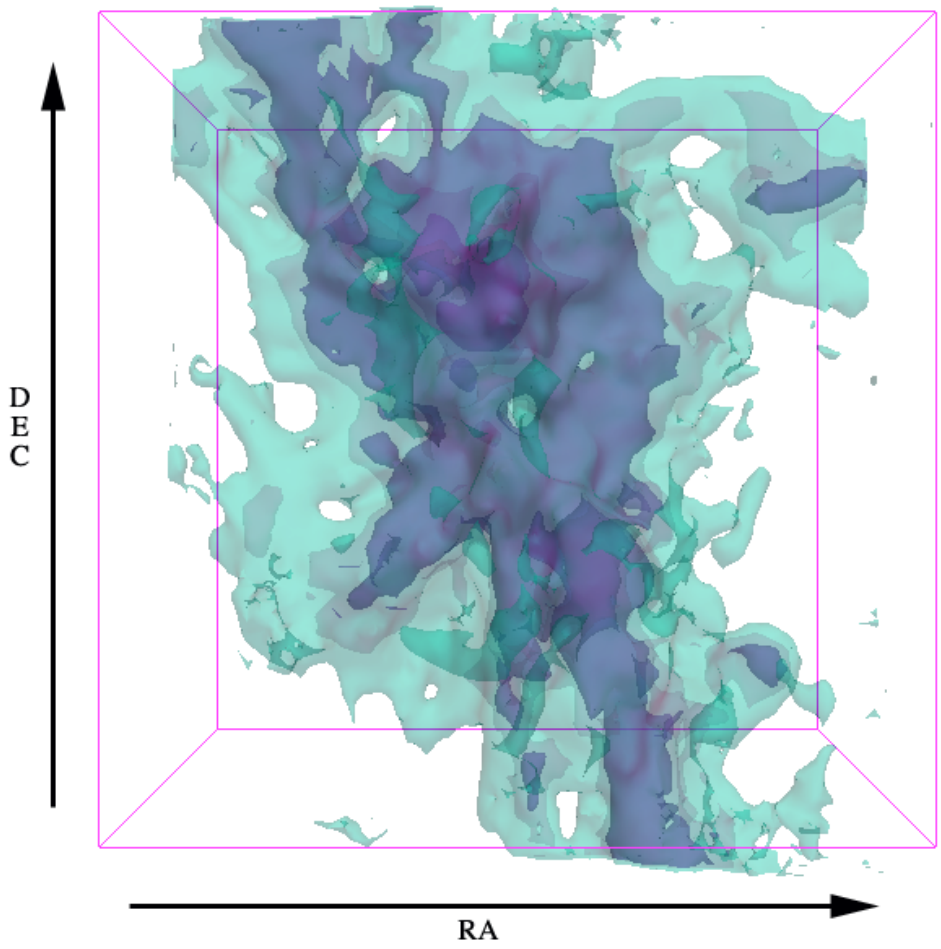

Figure 10: 3D contour models created in 3D Slicer of NGC 1333 in ^{13}CO.

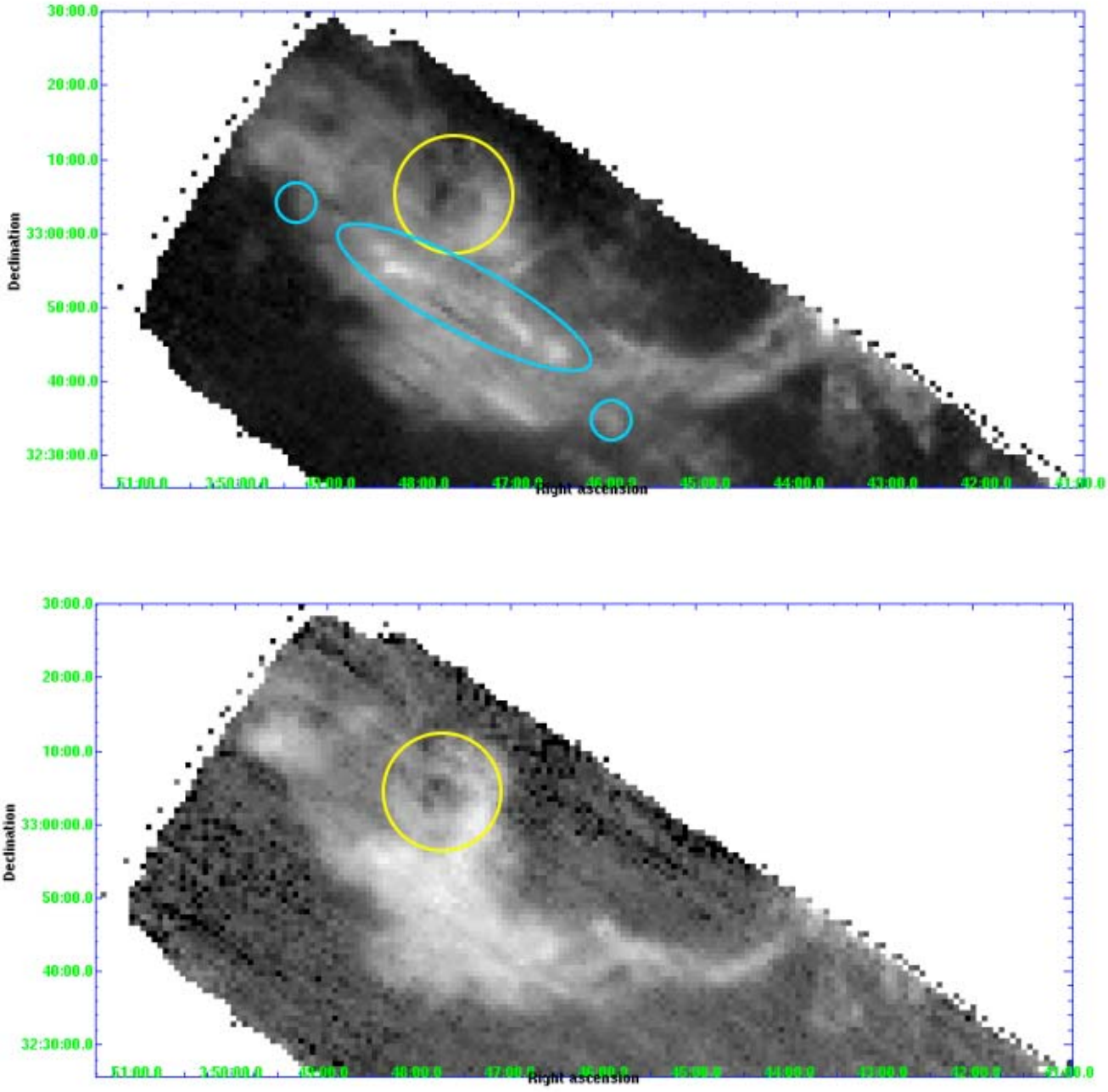

Figure 11: The top panel is a ^{12}CO integrated map of Region 1 (B5) with the IRS4 shell marked in yellow and the B5 outflow (including the proposed two new extensions) marked in teal. The bottom panel is a ^{13}CO integrated map of Region 1 (B5) with the IRS4 shell marked in yellow.

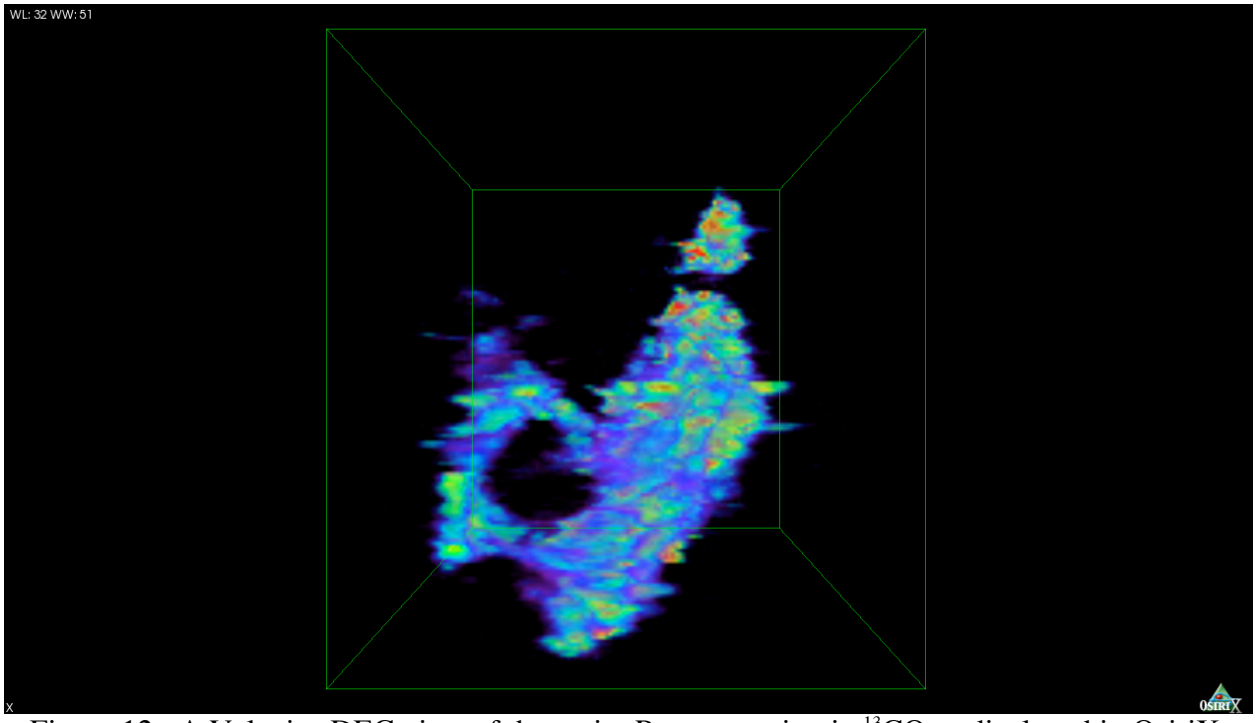

Figure 12: A Velocity-DEC view of the entire Perseus region in ^{13}CO as displayed in OsiriX. For more views of Perseus as displayed in OsiriX, see the Appendix.

4.1.2 Turbulence and Other Velocity Phenomena

Most of the topology of the isosurface models produced is determined by the kinematics and turbulence of the gas. There are many distinct velocity features visible in the 3D space that are not spikes from outflows or shells, but rather large blobs of high velocity gas or large clouds of gas at different velocities. One example of a high velocity blob of gas is visible in the B5 region as shown in Figure 13. This gas is highly red shifted, and not associated with any shell or outflow in the region. The cause of these phenomena is currently unexplained. Some examples of multiple clouds along the line of sight causing unusual velocity structure in the 3D models can be seen near B1, and some sample spectra are shown in Figure 14. These clouds are detectable in the spectra, but their distinct location in velocity space is dramatic in the OsiriX and 3D Slicer visualizations.

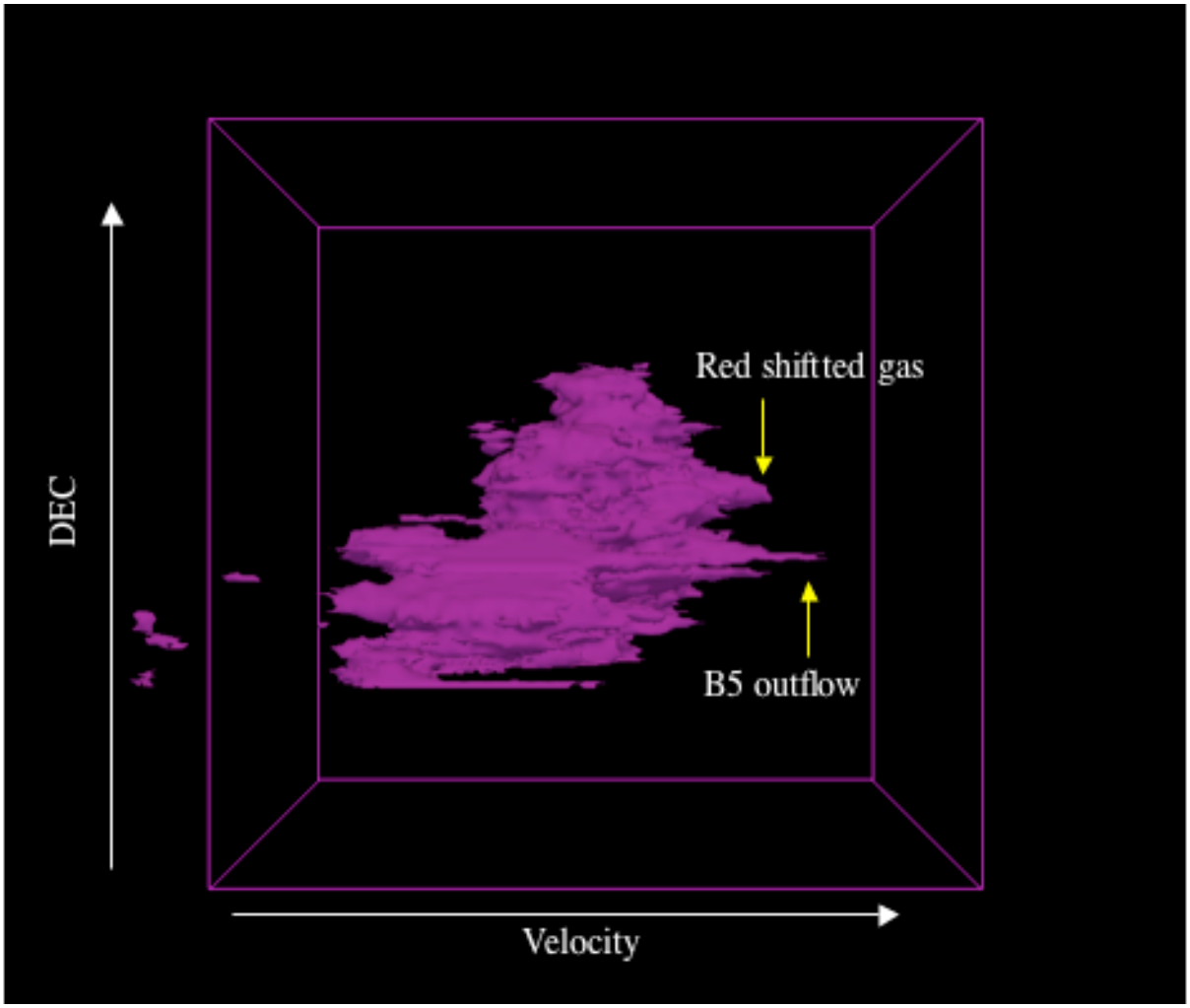

Figure 13: Velocity-DEC view of Region 1 3D Slicer model in ^{12}CO. The spike from the B5 outflow is marked, and a blob of highly red shifted gas is marked.

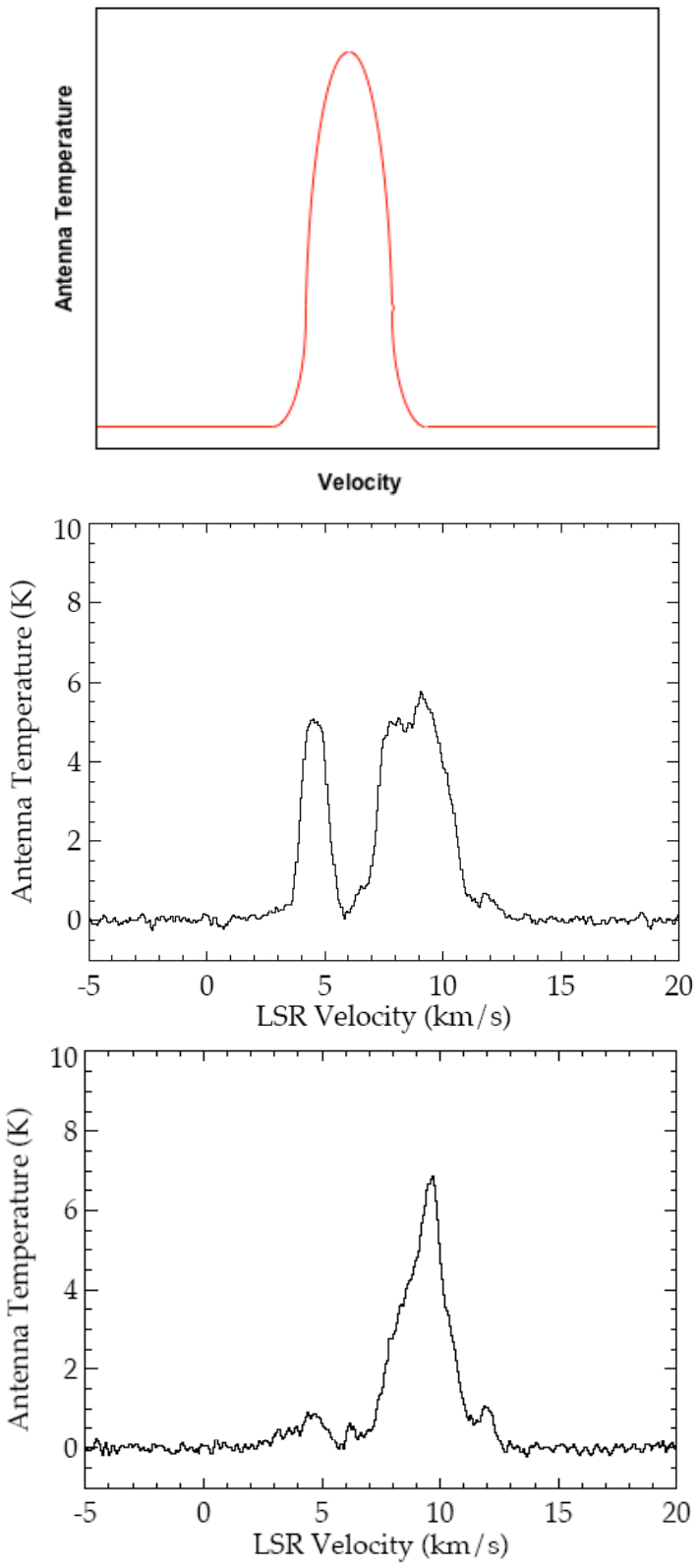

Figure 14: The top panel represents an idealized spectrum of a standard distribution of molecular gas. The two lower panels are integrated ^{12}CO spectra of points (located in Region 3 of Perseus) with no known associated velocity mechanism.

4.1.3 Outflows

The primary features focused on for this paper are the outflows in Perseus. As discussed in Section 3, the outflows appear in the form of sharp spikes when modeled in RA-DEC-Velocity space. Some sample spectra from known outflows are shown in Figure 15. Some of the outflow spectra are very clear and easy to identify such as the B5 outflow (middle panel), while others are buried within other emission and are less obvious (lower panel). When looking across all of Perseus, although the highest concentrations of outflows are in the known star forming regions such as IC 348 and NGC 1333, one can see outflows sticking out the entire length of the cloud. Worth noting is that the catalog of velocity points and outflows generated for this paper are most likely an underestimate of the true total number of outflows due to the resolution of the CO maps. Since the size of outflows in Perseus range greatly (from 0.1 to 5 pc), if the outflow is too small or weak, is located in a dense cluster of other outflows, or all of its emission is at the same velocity as the ambient gas, then it is hard to distinguish between the individual outflows on this scale. In order to better catalog the denser star forming regions, higher resolution data and separate models need to be generated to identify the smaller outflows. The technique used for identifying outflows in this research was optimized for being efficient at finding outflows across a large region which it proved to do very well.

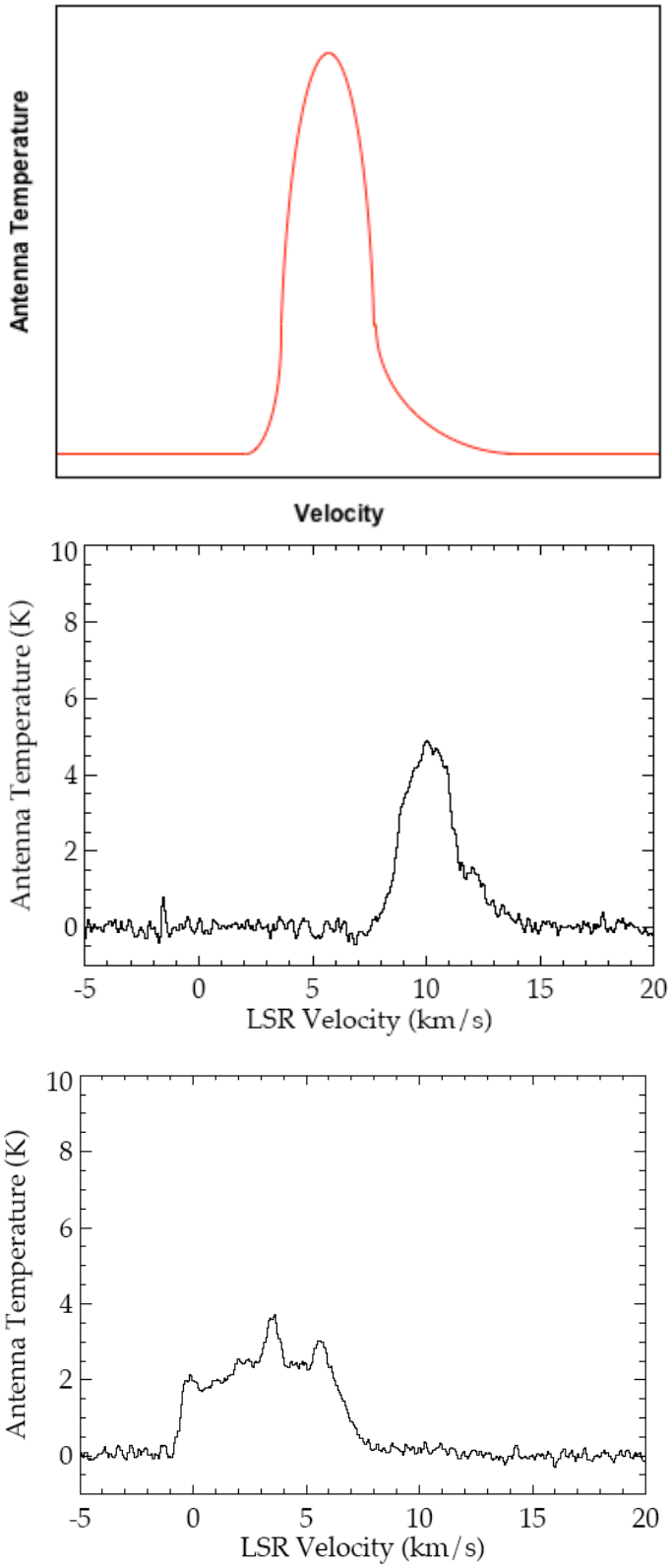

Figure 15: The top panel represents an idealized spectrum for the red shifted lobe of an outflow. The two lower panels are integrated ^{12}CO spectra of two actual red shifted outflow lobes found in Perseus (middle – B5, bottom – L1448).

4.2 B5 Detailed Study

The B5 region of Perseus was chosen for more detailed analysis because it is a very diverse region with lots of outflows, a shell, and interesting turbulent features, but is also simpler than the other regions of Perseus to understand due to the lack of multiple clouds along the line of sight. The dominant features of the region are the B5 outflow and the shell around IRS 4 as shown in Figure 11. The B5 outflow was well marked by the points from 3D Slicer (6 points), including two knots of gas (one point for each) which appear to be part of the outflow but previously unassociated with it (see Figure 11). This is not only visually evident since they line up with the outflow, but their spectra display strong red or blue wings. The other main feature of the region is IRS 4 which has a shell around it and an outflow as discussed in Section 4.1.1. There are 4 blue shifted and 4 red shifted points identified with 3D Slicer that may be associated with uncataloged outflows in this region. For each of these points and the points identified as being associated with known outflows, the mass, momentum, and kinetic energy was calculated as discussed in Section 3.3 for each area of gas for its specific velocity range (see Table 3 and Tables A5, A6, and A7 in the Appendix).

To determine the amount of high velocity gas in the region, the spectra for all of Region 1 were summed up and then was compared to a Gaussian fit as shown in Figure 16. A Gaussian fit was used because it is a good fit for a standard distribution of gas in a molecular cloud, and the cloud will have some high velocity components of gas so the wings on the Gaussian make physical sense (Falgarone & Phillips 1990; Schneider, et al. 1996). When determining what percent of the high velocity gas is contained in outflows, only the red wing of the spectrum was analyzed due to absorption features in the blue wing. This is because the OFF position for the survey was not emission free, so when looking at spectra in which there is low or no blue emission there will be a dip in the spectrum. This is visible in Figure 16. The spectra of blue shifted outflowing gas however will not display this absorption feature as well due to the high value of the blue emission. Thus calculations for the blue shifted velocity gas mass would be underestimates the amount of blue shifted ^{12}CO mass. This can be corrected in the future by extracting the spectrum for the OFF position from the raw OTF files, and then adding it to all the spectra in the map.

It appears that not all of the high velocity mass in the region is due to outflows. This is evident in Figure 16 in which the spectrum of the summation of all the spectra in the region are

Table 3: Kinematic statistics calculated for each point using Table A4 velocity ranges.

name	Mass Msolar	Momentum km/s	Kinetic energy 10^42 ergs
region1_B3	0.3	-0.53	9.42
region1_B4	0.3	-0.61	12.74
region1_B12	0.12	-0.29	6.94
region1_B15	0.48	-0.87	16.07
region1_B20	0.24	-0.43	7.77
region1_B22	0.26	-0.28	3.06
region1_B24	1.27	-0.151	18
region1_R0	0.89	1.55	28.27
region1_R1	0.56	1.09	21.95
region1_R2	0.08	0.1	1.32
region1_R6	0.04	0.07	1.17
region1_R10	0.09	0.17	3.2
region1_R12	0.14	0.15	1.55
region1_R14	0.1	0.17	2.88
region1_R17	0.92	1.36	20.49
region1_R18	0.35	0.48	6.67
region1_R19	0.16	0.23	3.18
region1_R20	0.17	0.29	5.25
region1_R21	0.07	0.08	1.05
totals:	6.54	2.579	170.980

plotted with the spectra representing the summation of the spectra for all the outflows in the region and just the previously identified outflows. The Gaussian was fitted to only the red shifted half and to the top 90% of the Region 1 summation spectra so as not to take the high velocity gas due to outflows and not normal turbulent processes into account. When calculating the red shifted high velocity mass, a velocity range of 11.9 to 13.3 km s^{-1} was used since 11.9 km s^{-1} is where the Gaussian drops below the summed spectra for Region 1, and 13.3 km s^{-1} is where the summed spectra for Region 1 dips below the Gaussian (drops into the baseline noise). This range is visible in Figure 17 which is a close-up of the red wing from Figure 16. The mass ratio for the outflowing gas was calculated from 12.68 to 13.3 km s^{-1}, and the mass ratio for previously detected outflows was calculated from 12.83 to 13.3 km s^{-1}. The high velocity gas associated with outflows account for about 10% and previously detected outflows account for about 6% of all the high velocity gas in the region. This number is consistent with estimates of 7-10% calculated for individual outflows and the gas in its immediate vicinity (Arce 2001). This implies that not all of the high velocity gas in the region is produced by detected outflows.

The mass ratio was also calculated for a subset of Region 1 to see if excess emission, low level noise, or other velocity gradients were affecting the percentages. A portion of Region 1 was used that does not include the area from RA = 3:45:0.336 to 3:41:0.523. This did not affect the percentages with the outflow mass still accounting for 10% of all the highly red shifted gas. All of these mass ratio estimates are underestimated because there is some high velocity gas from outflows past 13.3 km s^{-1}. However this mass was not included since the summation spectra for the whole region is only reliable up to 13.3 km s^{-1}. The missing high velocity mass may be in the form of undetected outflows that are either too small or too weak to be detected. There also may be extinct or episodic outflows that produced high velocity gas in the past but are now dormant or dead. Another possible source of this high velocity gas is in the form of highly turbulent gas, or high velocity blobs of gas like the one discussed in Section 4.1.2. The source of this high velocity gas is an important are for further investigation since it has implications for the distribution of gas velocities, the density of star formation, and the effects that outflows have on the molecular cloud even after the source has stopped producing outflowing gas.

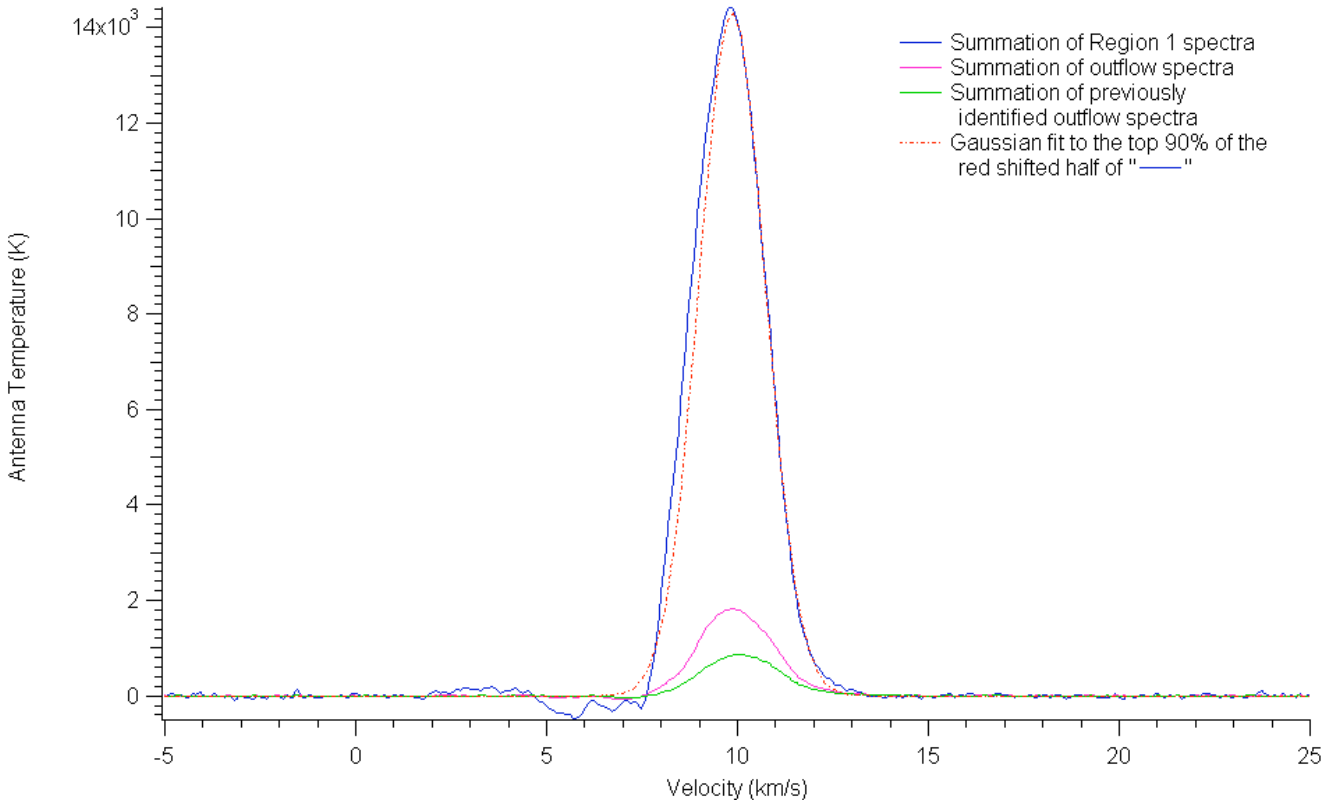

Figure 16: Summation of all the ^{12}CO spectra in Region 1 of Perseus (blue), the summation of all the spectra associated with the outflows in region 1 (pink), and the summation of all the spectra associated with only the previously identified outflows (green). A Gaussian fit to the top 90% of the red shifted half of the blue line is the dashed line.

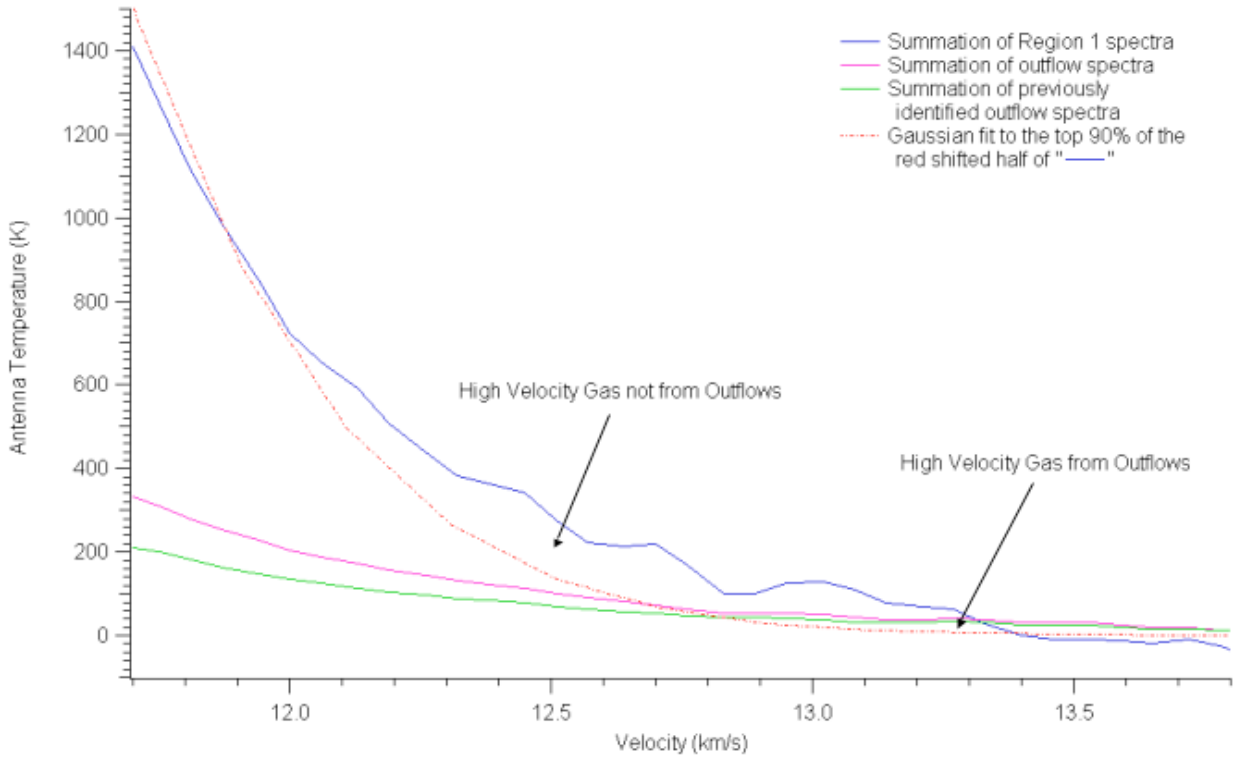

Figure 17: Plot focused on the red wings of the spectra in Figure 16. Summation of all the ^{12}CO spectra in Region 1 of Perseus (blue), the summation of all the spectra associated with the outflows in Region 1 (red), and the summation of all the spectra associated with only the previously identified outflows (green). The high velocity gas is the emission above the Gaussian.

5. Conclusion

A survey of all the high velocity features was conducted for Perseus using ^{12}CO and ^{13}CO molecular line maps from the COMPLETE Survey. 3D isosurface models created in 3D Slicer were used to detect high velocity gas from outflows in RA-DEC-Velocity space. Red and blue shifted points were cataloged for all six regions of Perseus, and three regions were further examined to determine which of the identified points were from outflows. In these three regions, one new shell was identified and 22 points associated with new outflows. One region, B5, was carefully studied and the mass, momentum, and kinetic energy was determined for each identified piece of gas that was associated with an outflow. The total amount of high velocity gas from outflows accounted for about 10% of all the high velocity gas in the region. The source of the remaining high velocity gas is yet to be determined.

Future work on this subject should include the full analysis, as done for Region 1 in this paper, for all the regions of Perseus. Also comparing the amount of mass contained in the high velocity points not identified as being from an outflow or shell would be enlightening as to whether this would account for some of the high velocity gas for the whole region. The necessary steps should also be taken to fix the error created by having an OFF position with blue shifted emission. Once this is corrected, more accurate mass estimates can be generated. Further investigation of this gas mass ratio will be valuable in understanding the outflow phase of a young star, how outflows affect the surrounding cloud, and the causes of velocity distribution of molecular clouds.

I would like to thank Alyssa Goodman as my thesis advisor, my academic advisor, and most importantly as a mentor. Alyssa's vision to merge visualization, astronomy, and medical imaging was the inspiration for this research. I would like to thank Héctor Arce for all his time and assistance which was invaluable to this research, and to Naomi Ridge who was always there with helpful guidance. Thanks to Michael Halle for being the bridge to the world of medical imaging and for his help on this research, to Erik Rosolowsky, David Wilner, and the entire COMPLETE team for all their input and feedback, and to Tom Laakso for the use of his data and for his collaboration.

References

Arce, Héctor, Ph.D. Thesis, Harvard University, 2001.

Aspin, C., Sandell, G., & Russell, A. P. G. 1994, A&AS, 106, 165

Borkin, Michelle A., Ridge, Naomi A., Goodman, Alyssa A., & Halle, Michael 2005, astro-ph/0506604

Bourke, Tyler L., Garay, Guido, Lehtinen, Kimmo K., Koehnenkamp, Ive, Launhardt, Ralf, Nyman, Lars-A., May, Jorge, Robinson, Garry, & Hyland, A. R. 1997, ApJ, 476, 781

Cernis, K. 1990, Ap&SS. 166, 315

Enoch, Melissa L., Young, Kaisa E., Glenn, Jason, Evans, Neal J., II, Golwala, Sunil, Sargent, Anneila I., Harvey, Paul, Aguirre, James, Goldin, Alexey, Haig, Douglas, Huard, Tracy L., Lange, Andrew, Laurent, Glenn, Maloney, Philip, Mauskopf, Philip, Rossinot, Philippe, & Sayers, Jack 2006, 638, 293

Falgarone, E. & Phillips, T. G. 1990, ApJ, 359, 344

Fallscheer, C., Borkin, M., Ridge, N., Schnee, S., & Goodman, A. 2003, AAS, 203, #77.02

Gering, D., Master's Thesis, Massachusetts Institute of Technology, 1999.

Gering, D., Nabavi, A., Kikinis, R., Eric, W., Grimson, L., Hata, N., Everett, P., Jolesz, F., & Wells III, W. "An Integrated Visualization System for Surgical Planning and Guidance using Image Fusion and Interventional Imaging." Medical Image Computing and Computer-Assisted Intervention (MICCAI), Cambridge England, 1999.

Goldsmith, P. F., Langer, W. D., & Wilson, R. W. 1986, ApJ, 303, 11

Herbig, G. H. & Jones, B. F. 1983, AJ, 88, 1040

Jorgensen, Jes K., Harvey, Paul M., Evans, Neal J., II, Huard, Tracy L., Allen, Lori E., Porras, Alicia, Blake, Geoffrey A., Bourke, Tyler L., Chapman, Nicholas, Cieza, Lucas, Koerner, David W., Lai, Shih-Ping, Mundy, Lee G., Myers, Philip C., Padgett, Deborah L., Rebull, Luisa, Sargent, Anneila I., Spiesman, William, Stapelfeldt, Karl R., van Dishoeck, Ewine F., Wahhaj, Zahed, & Young, Kaisa E. 2006, astro-ph/0603547

Lada, Elizabeth A. & Lada, Charles J. 1995, AJ, 109, 1682

Ladd, E. F., Lada, E. A., & Myers, P. C. 1993, ApJ, 410, 168

Luhman, K. L., Stauffer, John R., Muench, A. A., Rieke, G. H., Lada, E. A., Bouvier, J., & Lada, C. J. 2003, ApJ, 593, 1093

Margulis, M. & Lada, C. J. 1985, ApJ, 299, 925

Quillen, Alice C., Thorndike, Stephen L., Cunningham, Andy, Frank, Adam, Gutermuth, Robert A., Blackman, Eric G., Pipher, Judith L., & Ridge, Naomi 2005, ApJ, 632, 941

Ridge, Naomi A., Di Francesco, James, Kirk, Helen, Li, Di, Goodman, Alyssa A., Alves, João F., Arce, Héctor G., Borkin, Michelle A., Caselli, Paola, Foster, Jonathan B., Heyer, Mark H., Johnstone, Doug, Kosslyn, David A., Lombardi, Marco, Pineda, Jaime E., Schnee, Scott L., Tafalla, Mario 2006, astro-ph/0602542

Rohlfs, K., & Wilson, T. L. 1996, Tools of Radio Astronomy (Berlin: Springer)

Rosolowsky, Erik W., Goodman, Alyssa A., Wilner, David J., & Williams, Jonathan P. 1999, ApJ, 524, 887

Sargent, A. I. 1979, ApJ, 233, 163

Schneider, N., Stutzki, J., Winnewisser, G., & Blitz, L. 1996, ApJ, 468, 119

Wu, Y., Wei, Y., Zhao, M., Shi, Y., Yu, W., Qin, S., & Huang, M. 2004, A&A, 426, 503

Appendix

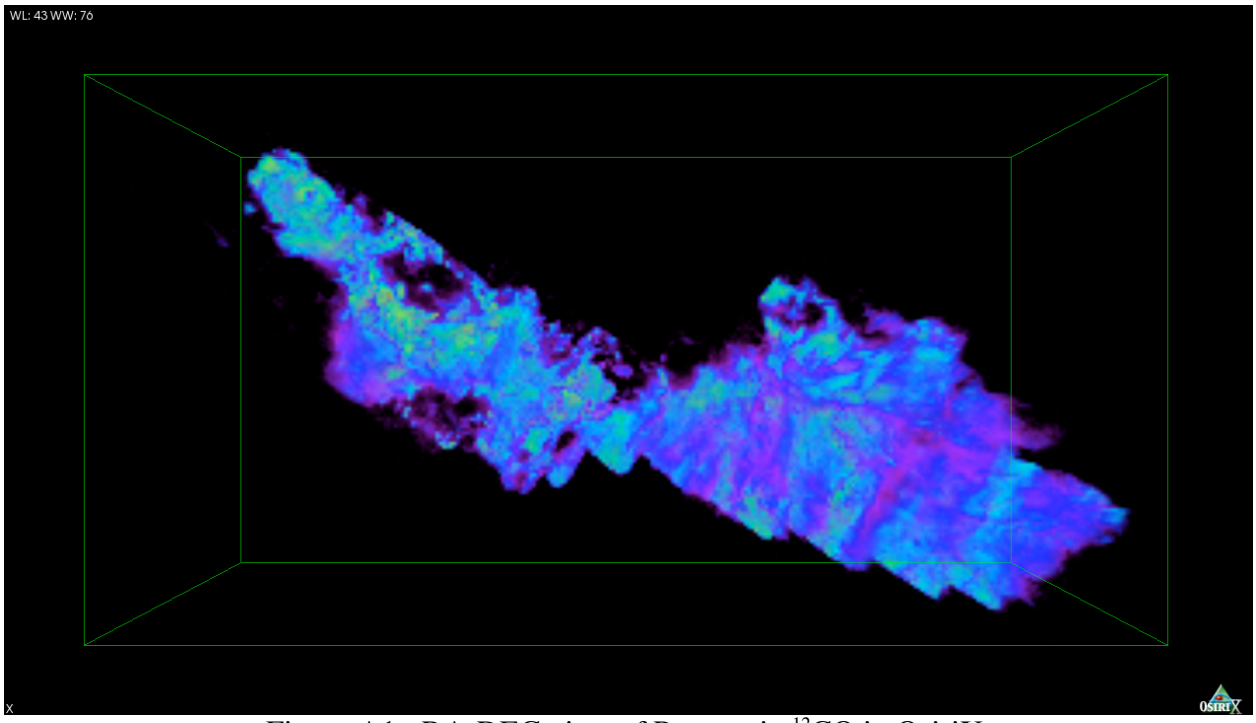

Figure A1: RA-DEC view of Perseus in ^{12}CO in OsiriX.

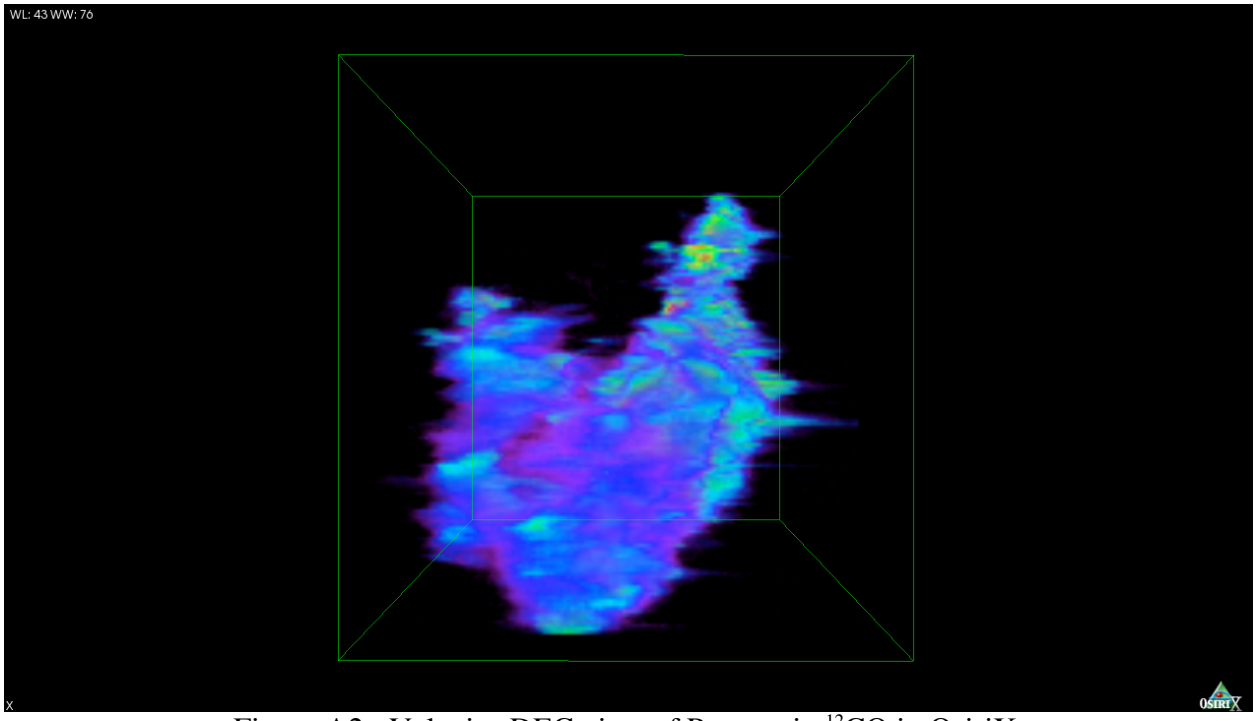

Figure A2: Velocity-DEC view of Perseus in ^{12}CO in OsiriX.

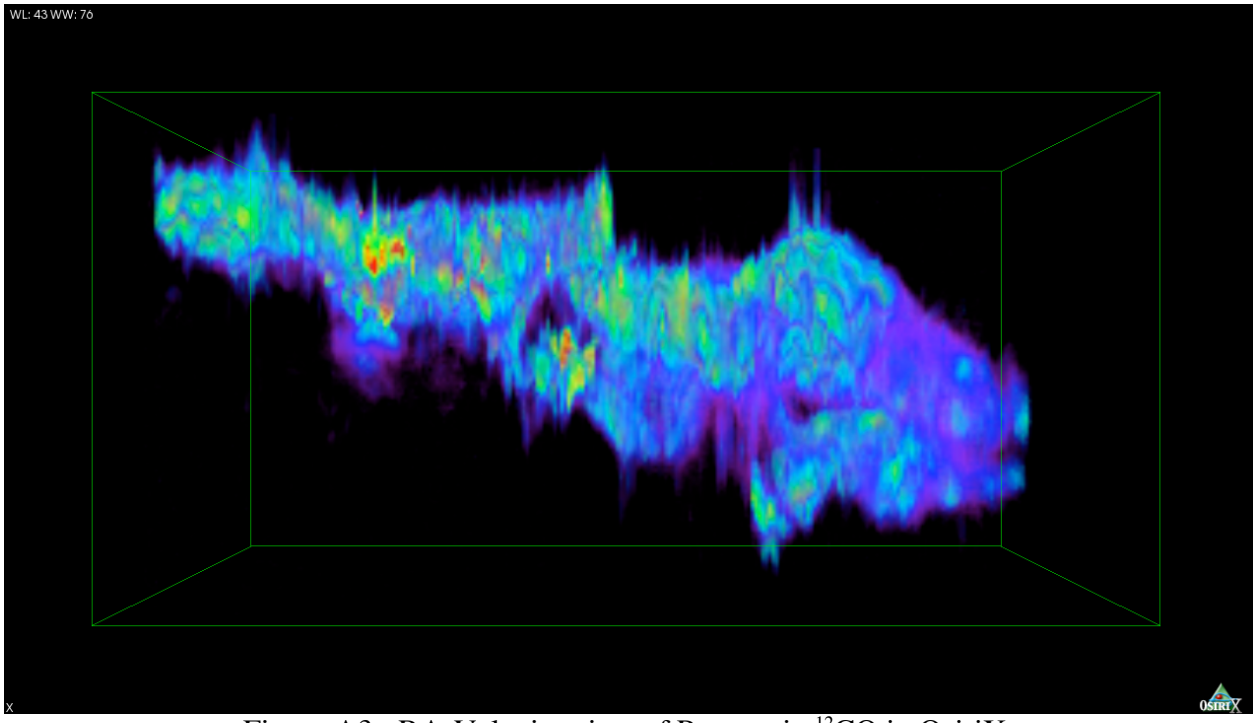

Figure A3: RA-Velocity view of Perseus in ^{12}CO in OsiriX.

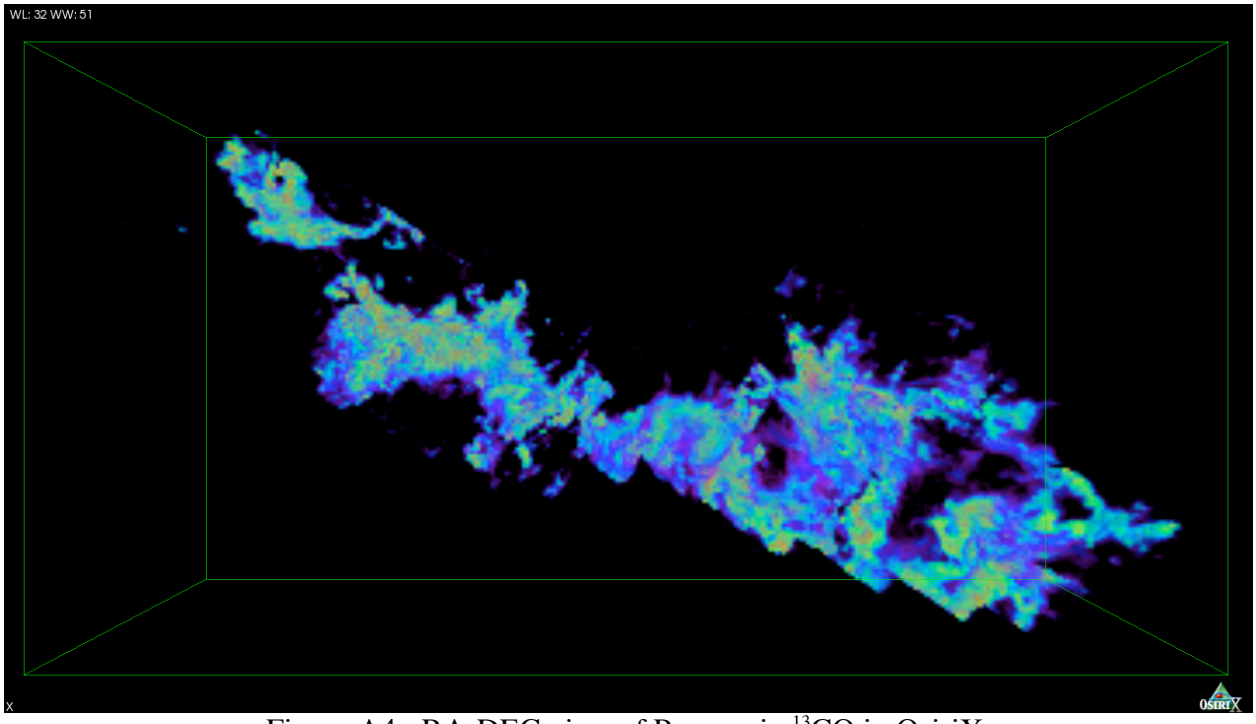

Figure A4: RA-DEC view of Perseus in ^{13}CO in OsiriX.

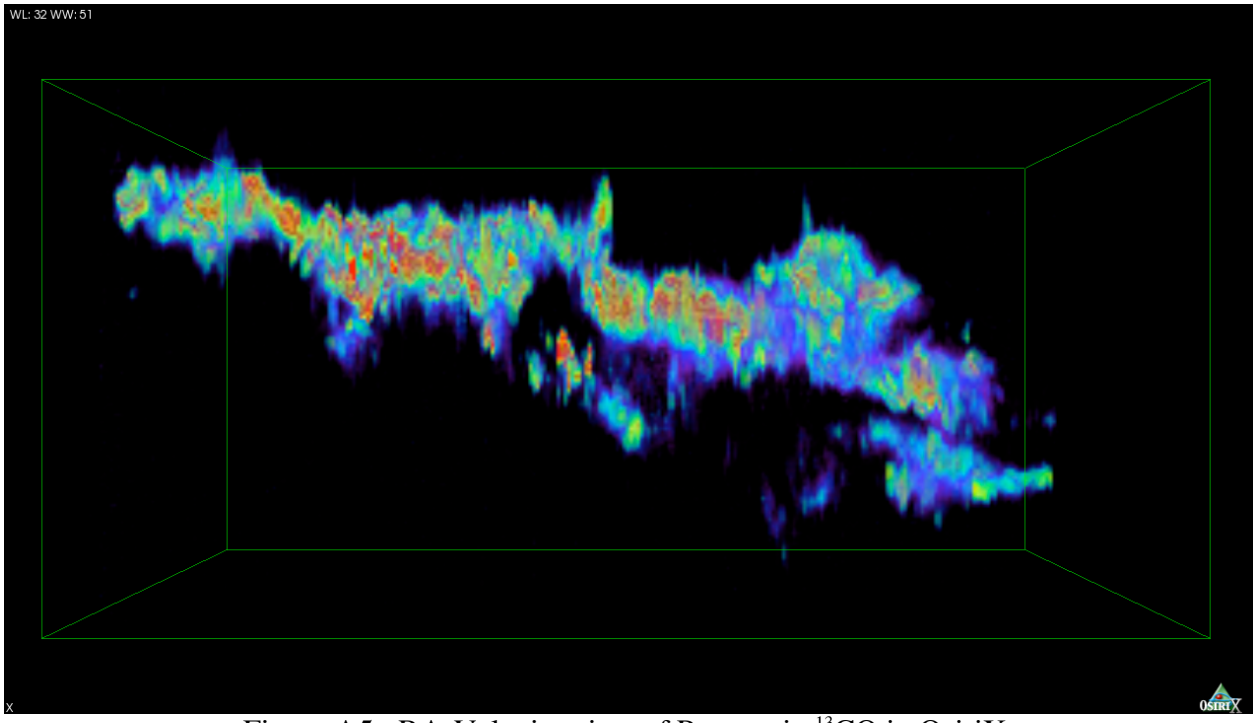

Figure A5: RA-Velocity view of Perseus in ^{13}CO in OsiriX.

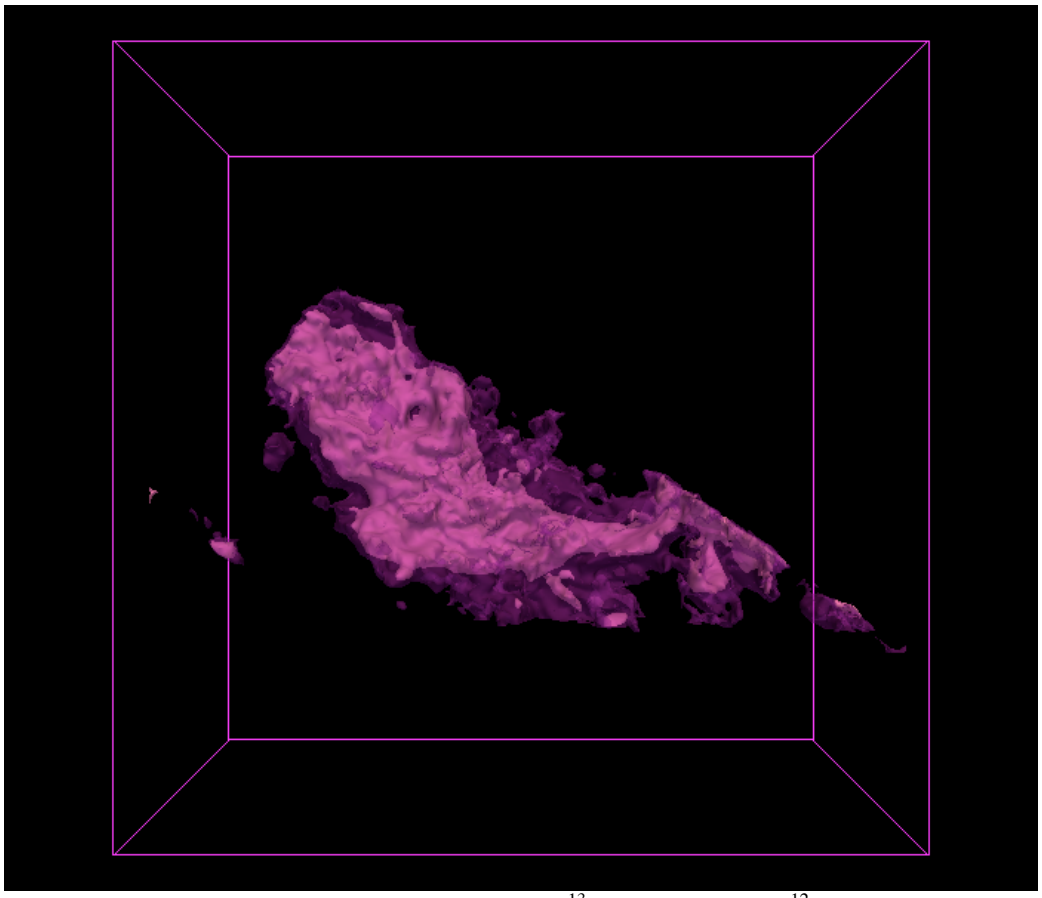
Figure A6: RA-DEC view of Region 1 with ^{13}CO in pink and ^{12}CO in light purple.

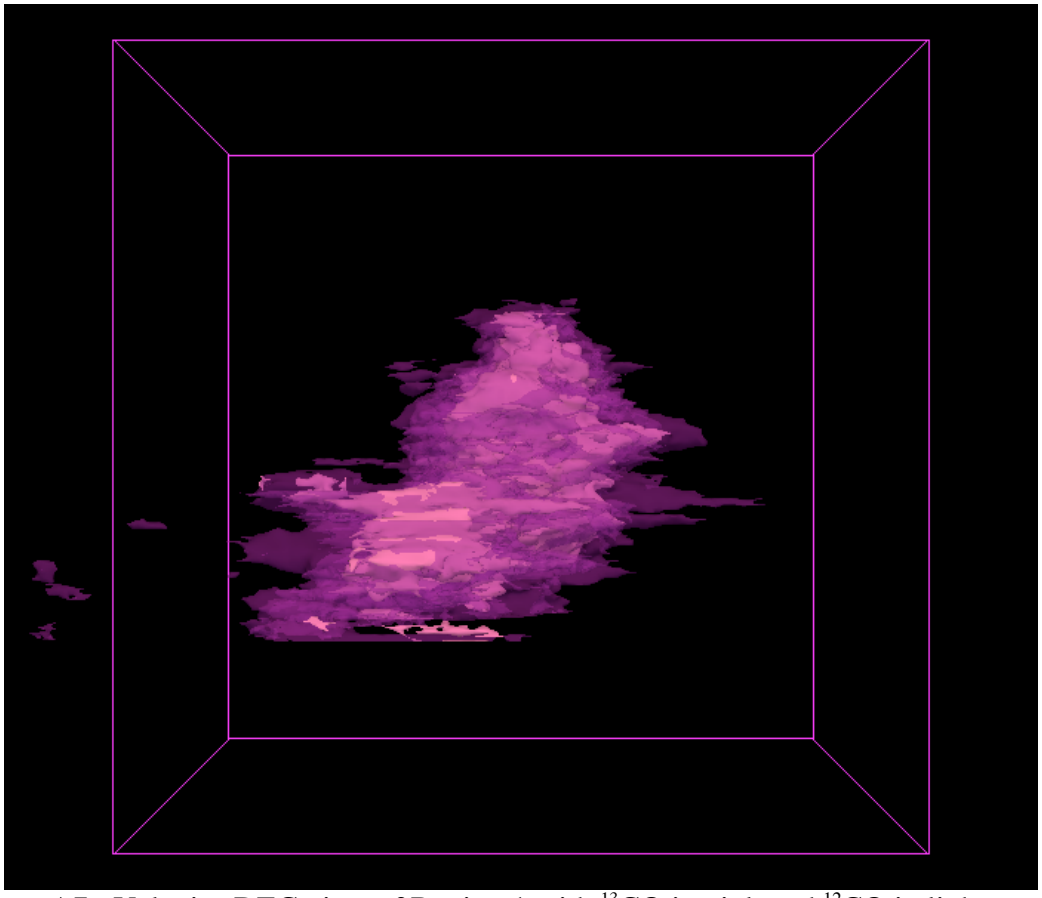

Figure A7: Velocity-DEC view of Region 1 with ^{13}CO in pink and ^{12}CO in light purple.

Table A1: Region corner locations in astronomical and pixel coordinates.

Region	Corner Locations RA	DEC	X	Y
1	57.88216	33.49	1	547
1	55.26986	33.49	342	547
1	55.29838	32.42944	342	381
1	57.87951	32.42944	1	381
2	57.34164	32.55722	72	401
2	54.6583	32.55722	426	401
2	54.71496	30.7875	426	124
2	57.34765	30.7875	72	124
3	54.8099	32.55722	406	401
3	53.52887	32.55722	575	401
3	53.62233	30.41694	575	66
3	54.87438	30.41694	406	66
4	53.68047	32.55722	555	401
4	52.58136	32.55722	700	401
4	52.69625	30.41694	700	66
4	53.7705	30.41694	555	66
5	53.03616	32.55722	640	401
5	51.24727	32.55722	876	401
5	51.41874	30.00167	876	1
5	53.1598	30.00167	640	1
6	51.73268	32.09083	816	328
6	50.04347	32.09083	1040	328
6	50.20885	30.00167	1040	1
6	51.86138	30.00167	816	1

Table A2: 3D Slicer model making settings.

Region	Threshold Intensity Lo	Hi	Remove Island Filter Minimum island size
1	25	255	10
2	15	255	10
3	20	255	10
4	20	255	10
5	10	255	10
6	30	255	10

Table A3: List of all the high velocity points identified in 3D Slicer.

MASTER LIST OF SLICER GENERATED POINTS

	ASTRONOMICAL (RA,DEC)					
	J2000	J2000 (deg)	J2000			J2000 (deg)
name	RA	RA	DEC			DEC
region1_B0	3 42 56.897	55.7370708	32	41	19.26	32.6886833
region1_B1	3 50 0.465	57.5019375	32	58	21.73	32.9727028
region1_B2	3 49 40.917	57.4204875	33	1	18.97	33.0219361
region1_B3	3 49 23.079	57.3461625	33	2	20.31	33.038975
region1_B4	3 48 18.933	57.0788875	32	54	55.1	32.9153056
region1_B5	3 48 9.68	57.0403333	32	33	53.85	32.5649583
region1_B6	3 44 24.148	56.1006167	32	47	24.59	32.7901639
region1_B7	3 44 12.554	56.0523083	32	49	3.46	32.8176278
region1_B8	3 43 54.187	55.9757792	32	49	22.41	32.8228917
region1_B9	3 43 18.17	55.8257083	32	28	17.06	32.4714056
region1_B10	3 43 40.476	55.91865	32	29	52.22	32.4978389
region1_B11	3 45 15.338	56.3139083	32	29	11.42	32.4865056
region1_B12	3 48 23.89	57.0995417	32	38	43.7	32.6454722
region1_B13	3 47 26.828	56.8617833	32	34	24.27	32.5734083
region1_B14	3 46 35.706	56.648775	32	27	13.07	32.4536306
region1_B15	3 45 58.399	56.4933292	32	42	31.78	32.7088278
region1_B16	3 44 53.611	56.2233792	32	32	19.87	32.5388528
region1_B17	3 45 46.127	56.4421958	33	0	28.45	33.0079028
region1_B18	3 48 40.355	57.1681458	33	24	40.03	33.4111194
region1_B19	3 48 34.518	57.143825	33	23	19.24	33.3886778
region1_B20	3 46 39.406	56.6641917	32	44	49.1	32.7469722
region1_B21	3 48 57.95	57.2414583	32	52	47.23	32.8797861
region1_B22	3 49 44.549	57.4356208	33	12	34.41	33.2095583
region1_B23	3 44 47.761	56.1990042	32	38	26.03	32.6405639
region1_B24	3 47 24.118	56.8504917	33	3	7.11	33.051975
region1_R0	3 47 0.942	56.753925	32	46	24.31	32.7734194
region1_R1	3 46 37.84	56.6576667	32	43	34.3	32.7261944
region1_R2	3 46 1.162	56.5048417	32	33	35.49	32.5598583
region1_R3	3 46 5.65	56.5235417	32	52	6.46	32.8684611
region1_R4	3 43 46.851	55.9452125	32	47	14.48	32.7873556
region1_R5	3 44 35.12	56.1463333	32	43	23.16	32.7231
region1_R6	3 47 18.211	56.8258792	32	38	41.2	32.6447778
region1_R7	3 47 19.34	56.8305833	32	58	36.93	32.976925
region1_R8	3 48 9.963	57.0415125	33	14	19.86	33.23885
region1_R9	3 49 9.344	57.2889333	33	18	1.36	33.3003778
region1_R10	3 47 3.748	56.7656167	32	55	16.88	32.9213556
region1_R11	3 50 11.697	57.5487375	33	7	5.57	33.1182139
region1_R12	3 47 3.007	56.7625292	32	35	10.48	32.5862444
region1_R13	3 49 19.173	57.3298875	32	57	19.33	32.9553694
region1_R14	3 47 53.633	56.9734708	33	1	54.34	33.0317611

region1_R15	3	49	21.174	57.338225	33	26	32.4	33.4423333
region1_R16	3	50	5.948	57.5247833	33	9	58.34	33.1662056
region1_R17	3	47	26.518	56.8604917	32	49	46.41	32.8295583
region1_R18	3	47	34.82	56.8950833	33	6	24.22	33.1067278
region1_R19	3	49	27.864	57.3661	33	12	31.22	33.2086722
region1_R20	3	48	34.244	57.1426833	32	58	24.19	32.9733861
region1_R21	3	45	32.974	56.3873917	32	43	11.93	32.7199806
region1_R22	3	44	5.616	56.0234	32	43	43.26	32.7286833
region1_R23	3	43	32.194	55.8841417	32	36	57.21	32.6158917
region1_R24	3	42	56.459	55.7352458	32	35	20.47	32.5890194
region1_R25	3	43	10.799	55.7949958	32	37	41.53	32.6282028
region1_R26	3	48	55.315	57.2304792	33	11	3.13	33.1842028
region1_R27	3	45	17.163	56.3215125	32	42	28.52	32.7079222
region1_R28	3	44	58.668	56.24445	32	37	33.4	32.6259444
region1_R29	3	43	44.945	55.9372708	32	45	1.42	32.7503944
region2_B0	3	43	16.673	55.8194708	31	38	46.31	31.6461972
region2_B1	3	41	24.621	55.3525875	31	40	1.39	31.6670528
region2_B2	3	40	18.714	55.077975	31	15	29.91	31.2583083
region2_B3	3	39	42.569	54.9273708	30	54	37.36	30.9103778
region2_B4	3	41	0.652	55.2527167	31	8	49	31.1469444
region2_B5	3	41	41.337	55.4222375	31	26	52.52	31.4479222
region2_B6	3	41	52.472	55.4686333	31	33	10.56	31.5529333
region2_B7	3	41	59.409	55.4975375	31	31	51.28	31.5309111
region2_B8	3	44	3.18	56.01325	32	5	10.86	32.08635
region2_B9	3	45	25.467	56.3561125	31	48	4.37	31.8012139
region2_B10	3	45	3.679	56.2653292	32	0	21.59	32.0059972
region2_B11	3	44	48.531	56.2022125	31	33	11.26	31.5531278
region2_B12	3	39	18.147	54.8256125	32	16	59.03	32.2830639
region2_B13	3	43	55.891	55.9828792	32	4	42.35	32.0784306
region2_B14	3	40	50.732	55.2113833	31	19	36.16	31.3267111
region2_B15	3	45	12.281	56.3011708	32	29	13.08	32.4869667
region2_B16	3	42	28.54	55.6189167	31	36	52.7	31.6146389
region2_R0	3	41	29.777	55.3740708	32	14	31.35	32.2420417
region2_R1	3	44	53.603	56.2233458	32	13	34.54	32.2262611
region2_R2	3	40	22.648	55.0943667	32	3	24.27	32.0567417
region2_R3	3	39	24.207	54.8508625	31	56	36.79	31.9435528
region2_R4	3	39	58.376	54.9932333	31	44	54.57	31.7484917
region2_R5	3	39	33.049	54.8877042	31	29	59.68	31.4999111
region2_R6	3	41	1.838	55.2576583	31	33	42.82	31.5618944
region2_R7	3	44	13.413	56.0558875	31	26	58.98	31.4497167
region2_R8	3	44	37.648	56.1568667	31	57	48.08	31.9633556
region2_R9	3	42	12.374	55.5515583	31	51	7.83	31.852175
region2_R10	3	41	40.606	55.4191917	32	1	12.63	32.020175
region2_R11	3	39	15.64	54.8151667	31	19	9.22	31.3192278
region2_R12	3	45	55.721	56.4821708	32	33	1.61	32.5504472
region2_R13	3	45	42.364	56.4265167	31	41	6.48	31.6851333

region2_R14	3	45	22.937	56.3455708	31	56	28.46	31.9412389
region2_R15	3	41	27.266	55.3636083	32	15	48.04	32.2633444
region2_R16	3	43	56.815	55.9867292	32	2	10.57	32.0362694
region2_R17	3	39	34.339	54.8930792	31	38	47.79	31.6466083
region2_R18	3	45	7.453	56.2810542	31	57	32.3	31.9589722
region3_B0	3	35	58.161	53.9923375	31	29	34.32	31.4928667
region3_B1	3	35	59.998	53.9999917	31	42	7.96	31.7022111
region3_B2	3	34	39.8	53.6658333	31	46	9.74	31.7693722
region3_B3	3	35	50.476	53.9603167	31	26	48.65	31.4468472
region3_B4	3	36	12.944	54.0539333	31	54	34.01	31.9094472
region3_B5	3	39	18.604	54.8275167	32	17	22.55	32.2895972
region3_B6	3	39	5.713	54.7738042	32	7	49.35	32.130375
region3_B7	3	39	2.437	54.7601542	32	3	19.93	32.0555361
region3_B8	3	38	0.33	54.501375	31	33	53.36	31.5648222
region3_B9	3	38	31.643	54.6318458	31	3	35.05	31.0597361
region3_B10	3	38	13.393	54.5558042	31	9	11.37	31.1531583
region3_B11	3	38	47.309	54.6971208	31	4	21.56	31.0726556
region3_B12	3	37	28.744	54.3697667	31	20	53.04	31.3480667
region3_B13	3	35	32.858	53.8869083	31	28	26.75	31.4740972
region3_B14	3	36	21.338	54.0889083	31	2	26.24	31.0406222
region3_B15	3	39	20.836	54.8368167	32	11	42.36	32.1951
region3_R0	3	36	56.1	54.23375	31	18	41.67	31.311575
region3_R1	3	36	33.968	54.1415333	31	32	39.01	31.5441694
region3_R2	3	37	44.698	54.4362417	31	24	29.59	31.4082194
region3_R3	3	36	49.178	54.2049083	31	38	10.06	31.6361278
region3_R4	3	38	12.245	54.5510208	31	54	15.31	31.9042528
region3_R5	3	39	24.32	54.8513333	31	56	42.67	31.9451861
region3_R6	3	38	59.295	54.7470625	32	5	29.5	32.0915278
region3_R7	3	37	31.808	54.3825333	31	32	32.42	31.5423389
region3_R8	3	38	4.438	54.5184917	31	30	12.63	31.5035083
region3_R9	3	37	54.939	54.4789125	31	32	41	31.5447222
region3_R10	3	39	27.722	54.8655083	32	10	35.68	32.1765778
region3_R11	3	39	25.225	54.8551042	32	17	29.39	32.2914972
region3_R12	3	39	9.879	54.7911625	31	19	4.58	31.3179389
region3_R13	3	36	23.529	54.0980375	31	27	42.14	31.4617056
region3_R14	3	37	39.379	54.4140792	31	46	27.49	31.7743028
region3_R15	3	36	57.071	54.2377958	31	27	42.25	31.4617361
region3_R16	3	34	49.854	53.707725	31	21	40.11	31.3611417
region3_R17	3	35	6.346	53.7764417	31	17	6.84	31.2852333
region3_R18	3	38	10.165	54.5423542	31	55	5.93	31.9183139
region3_R19	3	34	51.348	53.71395	31	1	36.06	31.0266833
region3_R20	3	35	17.874	53.824475	31	8	57.14	31.1492056
region3_R21	3	38	47.309	54.6971208	31	31	39.21	31.5275583
region4_B0	3	32	16.569	53.0690375	30	56	23.79	30.9399417
region4_B1	3	32	0.121	53.0005042	30	57	3.13	30.9508694
region4_B2	3	32	55.75	53.2322917	30	50	24.14	30.8400389

region4_B3	3	33	47.784	53.4491	30	55	1.31	30.9170306
region4_B4	3	30	36.77	52.6532083	31	57	2.77	31.9507694
region4_B5	3	30	57.816	52.7409	31	52	22.32	31.8728667
region4_B6	3	31	17.395	52.8224792	32	4	8.5	32.0690278
region4_B7	3	31	50.874	52.961975	31	12	48.5	31.2134722
region4_B8	3	30	49.636	52.7068167	30	36	0.9	30.60025
region4_B9	3	32	59.237	53.2468208	30	43	46.26	30.7295167
region4_B10	3	32	13.7	53.0570833	30	52	47.36	30.8798222
region4_B11	3	30	57.025	52.7376042	31	21	22.19	31.3561639
region4_R0	3	32	11.181	53.0465875	30	38	18.87	30.638575
region4_R1	3	31	39.465	52.9144375	30	53	47.4	30.8965
region4_R2	3	32	36.615	53.1525625	31	2	19.82	31.0388389
region4_R3	3	32	25.461	53.1060875	31	16	55.81	31.2821694
region4_R4	3	33	1.126	53.2546917	31	21	51.18	31.3642167
region4_R5	3	34	47.143	53.6964292	31	21	59.41	31.3665028
region4_R6	3	33	56.301	53.4845875	31	15	25.63	31.2571194
region4_R7	3	30	48.072	52.7003	31	33	39.37	31.5609361
region4_R8	3	30	19.55	52.5814583	31	26	39.22	31.4442278
region4_R9	3	34	49.131	53.7047125	31	1	42.85	31.0285694
region4_R10	3	33	39.718	53.4154917	31	29	27.17	31.4908806
region4_R11	3	33	19.172	53.3298833	30	59	1.7	30.9838056
region5_B0	3	26	52.894	51.7203917	30	17	4.95	30.2847083
region5_B1	3	32	14.679	53.0611625	30	55	49.47	30.9304083
region5_B2	3	25	34.851	51.3952125	30	28	33.29	30.4759139
region5_B3	3	25	28.176	51.3674	31	19	24.1	31.3233611
region5_B4	3	30	41.358	52.672325	31	55	59.35	31.9331528
region5_B5	3	30	58.808	52.7450333	31	51	6.39	31.851775
region5_B6	3	26	36.453	51.6518875	30	17	49.03	30.2969528
region5_B7	3	28	2.964	52.01235	31	48	16.67	31.8046306
region5_B8	3	25	3.319	51.2638292	31	1	45.35	31.0292639
region5_B9	3	25	10.399	51.2933292	31	14	51.42	31.2476167
region5_B10	3	28	34.721	52.1446708	31	9	6.7	31.1518611
region5_B11	3	28	37.424	52.1559333	31	12	49.6	31.2137778
region5_B12	3	28	53.256	52.2219	31	16	4.69	31.2679694
region5_B13	3	31	49.35	52.955625	31	12	11.6	31.2032222
region5_B14	3	27	31.273	51.8803042	31	6	56.75	31.1157639
region5_B15	3	26	42.91	51.6787917	31	5	49.94	31.0972056
region5_B16	3	28	50.487	52.2103625	30	55	7.19	30.9186639
region5_B17	3	29	2.061	52.2585875	30	43	44.34	30.7289833
region5_B18	3	28	15.821	52.0659208	31	4	3.53	31.0676472
region5_R0	3	29	55.637	52.4818208	31	5	7.56	31.0854333
region5_R1	3	28	16.151	52.0672958	31	0	39.76	31.0110444
region5_R2	3	32	9.007	53.0375292	30	38	0.43	30.6334528
region5_R3	3	29	36.644	52.4026833	31	17	39.8	31.2943889
region5_R4	3	29	46.474	52.4436417	31	20	13.96	31.3372111
region5_R5	3	30	49.906	52.7079417	31	33	50.49	31.564025

region5_R6	3	31	37.418	52.9059083	30	53	59.45	30.8998472
region5_R7	3	29	28.981	52.3707542	31	32	50.31	31.5473083
region5_R8	3	28	21.643	52.0901792	31	15	35	31.2597222
region5_R9	3	28	17.176	52.0715667	31	14	1.17	31.2336583
region5_R10	3	30	0.462	52.501925	31	27	23.42	31.4565056
region5_R11	3	28	48.002	52.2000083	31	26	14.04	31.4372333
region5_R12	3	29	9.445	52.2893542	31	23	36.57	31.3934917
region5_R13	3	28	24.721	52.1030042	31	8	30.93	31.141925
region5_R14	3	28	35.547	52.1481125	30	26	55.43	30.4487306
region5_R15	3	26	58.644	51.74435	30	17	43.24	30.2953444
region5_R16	3	27	55.438	51.9809917	31	19	22.82	31.3230056
region5_R17	3	28	21.342	52.088925	31	22	58.12	31.3828111
region5_R18	3	31	18.996	52.82915	31	42	27.43	31.7076194
region5_R19	3	25	34.855	51.3952292	30	41	6.34	30.6850944
region5_R20	3	25	38.653	51.4110542	30	36	35.19	30.609775
region5_R21	3	28	55.664	52.2319333	31	12	7.68	31.2021333
region5_R22	3	30	2.14	52.5089167	31	13	43.6	31.2287778
region5_R23	3	28	56.884	52.2370167	30	49	45.27	30.8292417
region6_B0	3	23	7.046	50.7793583	30	59	17.06	30.9880722
region6_B1	3	25	6.195	51.2758125	31	14	53.08	31.2480778
region6_B2	3	25	24.075	51.3503125	31	19	29.75	31.3249306
region6_B3	3	26	47.701	51.6987542	30	16	58.91	30.2830306
region6_B4	3	22	10.514	50.5438083	30	47	55.03	30.7986194
region6_B5	3	26	35.315	51.6471458	30	18	21.94	30.3060944
region6_B6	3	24	52.887	51.2203625	30	42	17.89	30.7049694
region6_B7	3	21	46.428	50.44345	30	37	55.87	30.6321861
region6_B8	3	21	13.402	50.3058417	30	35	15.28	30.5875778
region6_B9	3	23	31.955	50.8831458	30	25	19.91	30.4221972
region6_B10	3	22	54.28	50.7261667	30	6	18.76	30.1052111
region6_R0	3	26	55.727	51.7321958	30	17	0.42	30.28345
region6_R1	3	23	54.208	50.9758667	30	3	29.91	30.0583083
region6_R2	3	25	28.829	51.3701208	30	41	28.48	30.6912444
region6_R3	3	25	41.325	51.4221875	30	38	38.29	30.6439694
region6_R4	3	24	16.837	51.0701542	30	50	13.6	30.8371111
region6_R5	3	23	4.272	50.7678	31	3	9.4	31.0526111
region6_R6	3	23	25.714	50.8571417	30	50	6.35	30.8350972
region6_R7	3	25	16.832	51.3201333	30	44	31.24	30.7420111
region6_R8	3	27	19.493	51.8312208	30	32	51.48	30.5476333
region6_R9	3	26	43.679	51.6819958	31	17	8.79	31.285775

Table A4: Region 1 points associated with known outflows (blue highlight), unknown outflows (white), or shell (yellow).

	Pixel Dimensions				Velocity (channel number)	
name	xmin	ymin	xmax	ymax	min	max
region1_B3	34	48	39	55	280	292
region1_B4	50	38	54	41	257	288
region1_B12	51	17	53	20	272	280
region1_B15	90	20	94	25	270	290
region1_B20	78	23	82	27	276	293
region1_B22	29	61	32	63	293	300
region1_B24	68	49	72	52	291	299
region1_R0	71	26	76	31	338	363
region1_R1	79	23	83	25	342	370
region1_R2	90	9	93	14	334	341
region1_R6	68	16	72	19	340	347
region1_R10	72	38	74	40	343	352
region1_R12	74	12	77	13	330	336
region1_R14	60	47	62	49	340	348
region1_R17	65	30	70	34	336	349
region1_R18	64	53	69	55	335	344
region1_R19	33	60	37	63	337	342
region1_R20	48	41	52	44	338	377
region1_R21	96	22	100	25	332	341

Table A5: 13CO statistics for Region 1 outflow points.

name	Peak T K	Vo km/s	FWHM
region1_B3	0.80669	9.63506	1.1904
region1_B4	3.59553	10.0154	1.42235
region1_B12	1.15044	8.58612	1.18326
region1_B15	2.28654	9.81796	1.09619
region1_B20	2.84687	10.4807	1.43036
region1_B22	2.36167	10.0251	1.29287
region1_B24	2.2867	9.67664	1.50808
region1_R0	2.16294	10.212	1.56825
region1_R1	3.02335	10.4691	1.455
region1_R2	0.621734	9.63477	1.54547
region1_R6	2.20525	10.0717	1.42736
region1_R10	1.51599	10.4039	1.89406
region1_R12	1.11861	9.92006	1.3979
region1_R14	1.85935	10.5244	1.08449
region1_R17	3.60714	10.189	1.22054
region1_R18	2.85465	9.97928	0.933516
region1_R19	2.34703	10.1148	1.3192
region1_R20	2.2601	9.82601	1.51136
region1_R21	2.27031	9.67145	1.26477

Table A6: 12CO statistics for Region 1 outflow points.

	Tex			Peak antenna temp.			Vo			FWHM		
	Median	Mean	Std Dev	Median	Mean	Std Dev	Median	Mean	Std Dev	Median	Mean	Std Dev
name	K	K	K	K	K	K	km/s	km/s	km/s			
region1_B3	13.7928	13.107	2.06038	10.3921	9.72168	2.02239	9.47909	9.54387	0.272944	1.467	1.45133	0.186504
region1_B4	16.6374	16.6118	0.746572	13.2053	13.1802	0.739721	9.96873	9.95006	0.0887199	2.43618	2.48501	0.168482
region1_B12	13.8166	13.7213	0.750143	10.4155	10.3221	0.739646	8.69601	8.63197	0.0962182	1.46737	1.39677	0.215225
region1_B15	15.7117	15.4368	0.890562	12.2886	12.0171	0.880683	9.77763	9.76749	0.120688	1.75754	1.76083	0.122927
region1_B20	14.4554	14.4764	0.689536	11.0463	11.0673	0.681839	10.0865	10.1296	0.199865	2.71838	2.72403	0.377683
region1_B22	14.8744	14.9651	0.91508	11.4604	11.5506	0.904933	9.92108	9.933	0.0886083	1.83133	1.78583	0.153865
region1_B24	14.1183	13.9955	1.00614	10.7134	10.593	0.993043	9.98402	9.98345	0.0808189	2.49479	2.46257	0.248664
region1_R0	14.6364	14.6654	0.633088	11.2251	11.2541	0.625611	10.224	10.2126	0.158856	2.45297	2.52528	0.41347
region1_R1	14.4075	14.6836	1.08304	10.999	11.2726	1.07122	10.3025	10.2605	0.151857	2.83245	2.76724	0.505525
region1_R2	13.3322	12.5707	1.83337	9.93781	9.19221	1.8014	9.78685	9.80266	0.175048	1.90604	1.86976	0.225151
region1_R6	17.0337	17.1145	0.963583	13.598	13.6786	0.955642	10.0111	9.95775	0.118214	2.18688	2.1774	0.156637
region1_R10	15.0916	15.0661	0.264193	11.6751	11.6499	0.261214	10.4081	10.4186	0.088271	2.30233	2.36082	0.228705
region1_R12	17.4802	16.4705	1.88731	14.0408	13.0418	1.86935	9.95762	9.94137	0.0767526	1.9844	1.98106	0.1128
region1_R14	12.9785	12.9231	0.709804	9.5893	9.5352	0.698958	10.6335	10.6362	0.09322909	1.83377	1.8106	0.162724
region1_R17	15.4786	15.5676	0.781043	12.0579	12.1463	0.773027	10.0951	10.1145	0.111869	2.08477	2.08122	0.201523
region1_R18	14.6859	14.8107	0.923841	11.274	11.3979	0.913665	10.0637	10.046	0.136513	1.61448	1.55327	0.295214
region1_R19	14.9881	15.0142	0.423869	11.5727	11.5987	0.419101	10.1392	10.1293	0.0883786	1.91234	1.84813	0.143413
region1_R20	15.3314	15.3483	0.354616	11.9122	11.9291	0.350796	9.87029	9.86767	0.1152	2.801	2.31069	0.236703
region1_R21	15.0367	14.442	1.59138	11.6208	11.0351	1.57074	9.86125	9.84674	0.128076	1.99129	1.97166	0.0917721

Table A7: 13CO statistics for Region 1 outflow points.

	Peak antenna temp.			Vo			FWHM		
	Median	Mean	Std Dev	Median	Mean	Std Dev	Median	Mean	Std Dev
name	K	K	K	km/s	km/s	km/s			
region1_B3	1.85909	1.8007	0.607873	9.60564	9.61639	0.246064	0.92353	0.93722	0.15677
region1_B4	6.38613	6.3786	0.599679	10.0403	10.018	0.0737857	1.39866	1.4173	0.11968
region1_B12	2.30009	2.04232	0.521082	8.58541	8.58502	0.0962378	1.15207	1.10176	0.231733
region1_B15	4.44899	4.20935	1.11546	9.983141	9.79756	0.113854	1.07115	1.11717	0.240931
region1_B20	5.31758	5.18037	0.71584	10.4842	10.4937	0.0898844	1.38488	1.39076	0.143037
region1_B22	4.21815	4.12728	0.787481	10.0716	10.0397	0.0672207	1.32835	1.23208	0.243825
region1_B24	4.95335	4.46509	1.24067	9.66789	9.64772	0.143237	1.26426	1.34936	0.365395
region1_R0	4.39734	4.04666	1.23342	10.1536	10.1876	0.146924	1.53342	1.49934	0.140888
region1_R1	5.47617	5.27652	0.597656	10.4697	10.4753	0.0548979	1.46141	1.44322	0.146053
region1_R2	0.874081	1.24476	0.742414	9.73335	9.74057	0.222108	1.49084	1.54623	0.454232
region1_R6	4.18259	3.94251	1.13969	10.0974	10.0555	0.121937	1.45603	1.42102	0.0963623
region1_R10	2.67088	2.63295	0.352247	10.4303	10.4275	0.163052	1.79378	1.79026	0.32441
region1_R12	2.21777	1.83484	0.644298	9.92079	9.91846	0.0749162	1.38394	1.41768	0.180455
region1_R14	3.1803	3.19069	1.09278	10.5426	10.5502	0.104709	1.04971	1.03816	0.11934
region1_R17	6.55787	6.52938	0.285526	10.2147	10.193	0.0769685	1.21131	1.20977	0.0799625
region1_R18	5.58746	5.57501	0.611183	10.002	9.97045	0.129015	0.818966	0.833641	0.191435
region1_R19	4.32438	4.41292	0.711979	10.1394	10.105	0.156953	1.24476	1.21534	0.195017
region1_R20	3.81209	4.05223	1.2477	9.8022	9.81409	0.0932776	1.53868	1.51127	0.148678
region1_R21	4.3789	4.12635	1.29617	9.68959	9.6582	0.103333	1.16029	1.2166	0.1698